

# Reduced-dimensional vibrational models of the water dimer

Cite as: J. Chem. Phys. **156**, 164304 (2022); <https://doi.org/10.1063/5.0090013>

Submitted: 02 March 2022 • Accepted: 06 April 2022 • Accepted Manuscript Online: 07 April 2022 •

Published Online: 28 April 2022

 Emil Vogt,  Irén Simkó,  Attila G. Császár, et al.



View Online



Export Citation



CrossMark

## ARTICLES YOU MAY BE INTERESTED IN

[Highly accurate HF dimer ab initio potential energy surface](#)

The Journal of Chemical Physics **156**, 164305 (2022); <https://doi.org/10.1063/5.0083563>

[Adaptive fitting of potential energy surfaces of small to medium-sized molecules in sum-of-product form: Application to vibrational spectroscopy](#)

The Journal of Chemical Physics **156**, 164106 (2022); <https://doi.org/10.1063/5.0089570>

[Progress and perspectives in single-molecule optical spectroscopy](#)

The Journal of Chemical Physics **156**, 160903 (2022); <https://doi.org/10.1063/5.0087003>

Lock-in Amplifiers  
up to 600 MHz



Zurich  
Instruments



# Reduced-dimensional vibrational models of the water dimer

Cite as: J. Chem. Phys. 156, 164304 (2022); doi: 10.1063/5.0090013

Submitted: 2 March 2022 • Accepted: 6 April 2022 •

Published Online: 28 April 2022



View Online



Export Citation



CrossMark

Emil Vogt,<sup>1</sup> Irén Simkó,<sup>2,3</sup> Attila G. Császár,<sup>2,3</sup> and Henrik G. Kjaergaard<sup>1,a)</sup>

## AFFILIATIONS

<sup>1</sup>Department of Chemistry, University of Copenhagen, Universitetsparken 5, DK-2100 Copenhagen Ø, Denmark

<sup>2</sup>Laboratory of Molecular Structure and Dynamics, Institute of Chemistry, ELTE Eötvös Loránd University, Pázmány Péter Sétány 1/A, H-1117 Budapest, Hungary

<sup>3</sup>MTA-ELTE Complex Chemical Systems Research Group, P.O. Box 32, H-1518 Budapest 112, Hungary

<sup>a)</sup>Author to whom correspondence should be addressed: [hgk@chem.ku.dk](mailto:hgk@chem.ku.dk)

## ABSTRACT

A model based on the finite-basis representation of a vibrational Hamiltonian expressed in internal coordinates is developed. The model relies on a many-mode, low-order expansion of both the kinetic energy operator and the potential energy surface (PES). Polyad truncations and energy ceilings are used to control the size of the vibrational basis to facilitate accurate computations of the OH stretch and HOH bend intramolecular transitions of the water dimer ( $\text{H}_2^{16}\text{O}$ )<sub>2</sub>. Advantages and potential pitfalls of the applied approximations are highlighted. The importance of choices related to the treatment of the kinetic energy operator in reduced-dimensional calculations and the accuracy of different water dimer PESs are discussed. A range of different reduced-dimensional computations are performed to investigate the wavenumber shifts in the intramolecular transitions caused by the coupling between the intra- and intermolecular modes. With the use of symmetry, full 12-dimensional vibrational energy levels of the water dimer are calculated, predicting accurately the experimentally observed intramolecular fundamentals. It is found that one can also predict accurate intramolecular transition wavenumbers for the water dimer by combining a set of computationally inexpensive reduced-dimensional calculations, thereby guiding future effective-Hamiltonian treatments.

Published under an exclusive license by AIP Publishing. <https://doi.org/10.1063/5.0090013>

## I. INTRODUCTION

For more than half a century, vibrational spectroscopy of the water dimer, ( $\text{H}_2\text{O}$ )<sub>2</sub>, has been of interest from both experimental<sup>1–9</sup> and theoretical<sup>10–29</sup> aspects. In the dimer, the  $\text{H}_2\text{O}$  monomers are held together by an  $\text{OH}\cdots\text{O}$  hydrogen bond, considered to be the archetype of hydrogen bonds.<sup>30</sup> Within the many-body-expansion approach, the interaction of the two water monomers provides the leading contribution to potential energy surfaces (PESs) of larger water clusters.<sup>18,29</sup>

Similar to other weakly bound complexes, understanding the low-energy states of the water dimer is complicated by large-amplitude motions and, in particular, by complex splitting patterns caused by low-energy barriers. Developing the ability to compute these observable splittings has been an important goal of theoretical and computational spectroscopies.<sup>14,27,31,32</sup> For the water dimer, there are eight versions<sup>32</sup> of its equilibrium structure, of

$C_s$  point-group symmetry, if the possibility to break the four covalent OH bonds is ignored. The eight versions, corresponding to different numberings of the identical nuclei, can be interconverted by the so-called “tunneling” rearrangements, defining “donor-tunneling,” “acceptor-tunneling,” and “donor-acceptor interchange” paths.<sup>32</sup> The low-energy vibrational-rotational tunneling (VRT) states of the water dimer are sensitive to minor changes in the PES; thus, they provide important checks for modeling efforts.<sup>12</sup> The benchmark of computed line lists against experimentally observed transition wavenumbers provides another accurate measure of the quality of the PES. As a result, there are several studies<sup>12,20</sup> that have been designed to observe and assign VRT states. Due to its importance and its complex nuclear dynamics, different theoretical and computational approaches, including variational(-type) nuclear-dynamics computations, have been tested for the water dimer. The HBB,<sup>16</sup> HBB2,<sup>17,18</sup> WHBB,<sup>18</sup> MB-pol,<sup>20</sup> and CCpol-8si<sup>19,23</sup> PESs are examples of water-dimer potentials that

allow for displacements along all 12 vibrational degrees of freedom (DoF). VRT levels have been computed with each of these PESs.

Computation of VRT states is reported in Ref. 19 based on the CCpol-8sf PES (which was renamed to CCpol-8sfIR[2012] in Ref. 23). The authors of Ref. 19 used a (6 + 6)-dimensional (6D + 6D) adiabatic approach, in which the six high-energy (small-amplitude) intramolecular DoFs were separated from the six low-energy (large-amplitude) intermolecular DoFs. For the water dimer, and for its fully deuterated analog, this adiabatic approach resulted in accurate VRT energy levels.<sup>19</sup> At the same time, relatively large discrepancies from experiments were observed for the high-energy intramolecular transitions. The source of these discrepancies was not determined. More recently, numerically exact 12-dimensional (12D) calculations of the VRT levels, also based on the CCpol-8sf PES, were performed up to the region of the HOH bend states.<sup>27</sup> The (6D + 6D) and 12D results were in excellent agreement with each other and with experiments for the low-lying intermolecular energy levels, confirming that the adiabatic approximation is excellent in the low-energy region.<sup>19,27</sup> However, large differences (up to 11 cm<sup>-1</sup>) between the 12D and (6D + 6D) calculations were found for the bending fundamentals, implying a breakdown of the adiabatic approximation for the intramolecular transitions. Due to the rapidly increasing density of states, the 12D calculations could not be extended to the region of the OH-stretch fundamentals.<sup>27</sup>

Here, the focus is not on the low-energy VRT states but rather on the modeling of OH stretch and HOH bend *intramolecular* vibrational transitions of the water dimer. The formation of the hydrogen bond redshifts and increases the intensity of the bound OH stretch, OH<sub>b</sub>, fundamental transition. These hydrogen bond characteristics were captured in the early anharmonic local mode effective Hamiltonian calculations.<sup>13,33,34</sup> Later, the inclusion of intermolecular low-energy modes that partially break the hydrogen bond was found to affect the size of the redshift.<sup>22,24,35</sup> As a consequence, to calculate accurate intramolecular transitions with an effective Hamiltonian, one needs a good description of both the intramolecular and intermolecular modes, as well as the coupling between the two sets of modes. However, it is not obvious which types of approximations are suitable to calculate accurate intramolecular transitions from an effective Hamiltonian.

To address this question, we have developed a novel, flexible finite-basis representation (FBR) model based on a many-mode expansion of both the PES and the **G** matrix elements in the vibrational kinetic energy operator expressed in internal coordinates. The model and the associated code are termed VibMEMIC, in reference to its main characteristics: **V**ibrational **M**any-mode **E**xpansion **M**odel in **I**nternal **C**oordinates. With VibMEMIC, we perform a set of reduced-dimensional calculations to investigate the transition wavenumber shifts caused by the interaction between the intramolecular and intermolecular modes. Results are presented for VibMEMIC, as well as from computations performed with a discrete-variable-representation-based model, GENIUSH (**G**eneral code with **N**umerical, **I**nternal-coordinate, **U**ser-Specified **H**amiltonians),<sup>36-38</sup> in which neither the PES nor the kinetic energy operator is approximated. We used a newly calculated coupled-cluster singles, doubles and perturbative triples [CCSD(T)]-F12a/cc-pVTZ-F12 PES, abbreviated as F12, with VibMEMIC and the CCpol-8sfIR<sup>19,23</sup> and the MB-pol<sup>20</sup> surfaces with GENIUSH. We

discuss the degree to which the transition wavenumber shifts caused by each of the low-energy intermolecular modes are additive. In addition, we provide accurate intramolecular transition wavenumbers from full-dimensional 12D computations performed with VibMEMIC. We show that not only do the reduced-dimensional calculations provide physical insights into the transition wavenumber shifts but they can also predict the intramolecular transitions rather accurately.

## II. VibMEMIC

The VibMEMIC model was developed for the purpose of calculating accurate stretch and bend intramolecular transitions for hydrogen bound complexes. Most previous vibrational models focus either on the low-energy intermolecular modes or on the high-energy intramolecular modes. In earlier work, the coupling between the two sets of modes have typically been approximated or neglected. Models based on an adiabatic separation of the two sets of modes have proven useful for describing the effect of the intramolecular modes on the intermolecular transitions; however, this separation has been shown to work less well for the intramolecular transitions.<sup>19,27</sup> Models built on effective Hamiltonians can yield accurate intramolecular transitions for hydrogen bound complexes, but often these types of models rely to some extent on cancellation of error. Their accuracy depends on both the type of transitions and the validity of the introduced approximation for the specific complex in question.<sup>22,24</sup> The VibMEMIC model may be viewed as an extension of the effective Hamiltonian approaches to include a more accurate description of the low-energy intermolecular modes and their coupling with the high-energy intramolecular modes. Alternatively, it can be viewed as a reduction of the exact or near-exact models, typically used for the intermolecular modes, to facilitate calculations including more vibrational modes. In Sec. II A, the general framework for constructing the Hamiltonian in the VibMEMIC model is introduced. In Secs. II B–II E, we describe the employed coordinate system for the water dimer, general symmetry aspect of the water dimer and how symmetry is utilized, how the basis is truncated, and the employed notation for the intramolecular transitions, respectively.

### A. The Hamiltonian

The current version of VibMEMIC can solve only the vibrational Schrödinger equation, i.e., rotations are not treated. The *M*-dimensional vibrational Hamiltonian is expressed in the form derived by Podolsky,<sup>39</sup>

$$\hat{H} = \frac{1}{2} \sum_{ij}^M \tilde{g}^{-1/4} \hat{p}_i^\dagger G_{ij} \tilde{g}^{1/2} \hat{p}_j \tilde{g}^{-1/4} + V, \quad (1)$$

where *M* is the number of vibrational modes [ $M \leq 3N - 6(5)$ , and *N* is the number of atoms in the molecule],  $\hat{p}_i = -i\hbar \frac{\partial}{\partial q_i}$ , with *q<sub>i</sub>* being the *i*th coordinate, and  $\tilde{g} = \det(\mathbf{g})$ . The  $3N \times 3N$ -dimensional **g** and **G** matrices (covariant and contravariant metric tensors, respectively) can be expressed as<sup>40</sup>

$$g_{ij} = \sum_{\alpha=1}^{3N} m_{\alpha} \frac{\partial x_{\alpha}}{\partial q_i} \frac{\partial x_{\alpha}}{\partial q_j} \Leftrightarrow \mathbf{g} = \mathbf{J} \mathbf{M} \mathbf{J}^T \quad (2)$$

and

$$G_{ij} = \sum_{\alpha=1}^{3N} \frac{1}{m_{\alpha}} \frac{\partial q_i}{\partial x_{\alpha}} \frac{\partial q_j}{\partial x_{\alpha}} \Leftrightarrow \mathbf{G} = \mathbf{g}^{-1}, \quad (3)$$

where the sum is over all Cartesian coordinates of the atoms of the molecule,  $m_{\alpha}$  denotes the associated masses, the  $q_i$  coordinates include all vibrational, rotational, and translational coordinates,  $\mathbf{J}$  is the Jacobian matrix ( $J_{i\alpha} = \frac{\partial q_i}{\partial x_{\alpha}}$ ), and  $\mathbf{M}$  is the mass matrix ( $M_{\alpha\beta} = m_{\alpha} \delta_{\alpha\beta}$ ). The matrix  $\mathbf{G}$  is obtained by inverting  $\mathbf{g}$ , with elements of the Jacobian calculated using the finite-difference method. The Jacobian is of size  $3N \times 3N$ , and a full internal-coordinate definition, including the three rotational and three translational coordinates, is therefore required even for the reduced-dimensional vibrational models. The volume element of integration is  $d\tau = dq_1 dq_2 \dots dq_M$  (Wilson's normalization), for which the  $\hat{p}_i$  operator is Hermitian. We use  $\tilde{g} = \tilde{J}^2 \tilde{M}$  [Eq. (2)] and write the Podolsky form of the Hamiltonian as

$$\hat{H} = \frac{1}{2} \sum_{ij} \tilde{J}^{-1/2} \hat{p}_i^{\dagger} G_{ij} \tilde{J} \hat{p}_j \tilde{J}^{-1/2} + V. \quad (4)$$

In reduced dimensional models, where  $M < 3N - 6$ , there are constrained vibrational coordinates. These constraints can be taken into account either by deleting the corresponding rows and columns of  $\mathbf{g}$  and then inverting it to obtain  $\mathbf{G}$  or by inverting the full  $\mathbf{g}$  matrix and deleting the corresponding rows and columns of  $\mathbf{G}$ .

The vibrational basis functions in VibMEMIC are defined as products of eigenfunctions of 1D Hamiltonians ( $\hat{h}_i$ ). These 1D Hamiltonians describe each mode as being decoupled from the remaining vibrational modes,

$$\hat{h}_i = \frac{1}{2} \tilde{J}^{-1/2} \hat{p}_i^{\dagger} G_{ii} \tilde{J} \hat{p}_i \tilde{J}^{-1/2} + V_i^{(1D)}(q_i), \quad (5)$$

where  $G_{ii}$  is evaluated at the reference value of all other vibrational coordinates and  $V_i^{(1D)}(q_i)$  is the PES along the  $i$ th mode from the reference geometry. Details on the 1D Hamiltonians, the chosen basis functions, and the selected types of quadrature can be found in the [Appendix](#).

To evaluate integrals needed to solve the  $M$ -dimensional Schrödinger equation, both the elements of the  $\mathbf{G}$  matrix and the PES are represented with a many-mode expansion, truncated at third order,

$$\begin{aligned} V(q_1, q_2, \dots, q_M) &= V(q_1^{\text{ref}}, q_2^{\text{ref}}, \dots, q_M^{\text{ref}}) \\ &+ \sum_i^M V_i^{1D}(q_i) + \sum_{i<j}^M V_{ij}^{2D}(q_i, q_j) \\ &+ \sum_{i<j<k}^M V_{ijk}^{3D}(q_i, q_j, q_k) \end{aligned} \quad (6)$$

with

$$V_i^{1D}(q_i) = V(q_1^{\text{ref}}, q_2^{\text{ref}}, \dots, q_i, \dots, q_M^{\text{ref}}) - V(q_1^{\text{ref}}, q_2^{\text{ref}}, \dots, q_M^{\text{ref}}) \quad (7)$$

and

$$\begin{aligned} V_{ij}^{2D}(q_i, q_j) &= V(q_1^{\text{ref}}, q_2^{\text{ref}}, \dots, q_i, \dots, q_j, \dots, q_M^{\text{ref}}) \\ &- V(q_1^{\text{ref}}, q_2^{\text{ref}}, \dots, q_M^{\text{ref}}) - V_i^{1D}(q_i) - V_j^{1D}(q_j) \end{aligned} \quad (8)$$

and likewise for  $V_{ijk}^{3D}(q_i, q_j, q_k)$ , i.e., with  $V(q_1^{\text{ref}}, q_2^{\text{ref}}, \dots, q_M^{\text{ref}})$ , the 1D and the 2D surfaces involving the  $i$ th,  $j$ th, and  $k$ th mode subtracted from the 3D cut of the full PES from the reference geometry.

In this work, a new CCSD(T)-F12a/cc-pVTZ-F12<sup>41,42</sup> (abbreviated as F12) PES was calculated with the Molpro2020 program.<sup>43</sup> The CCSD(T)-F12a/cc-pVTZ-F12 calculations were performed with the recommended correlation factor of  $\beta = 1.0$ , the frozen core approximation, and default convergence criteria.<sup>41,42</sup> For the 1D, 2D, and 3D PES cuts, we use the displacement ranges given in Table S1 with a step size of  $5^\circ/0.05 \text{ \AA}$ ,  $10^\circ/0.10 \text{ \AA}$ , and  $15^\circ/0.15 \text{ \AA}$ , respectively. The PES was subsequently evaluated at the respective quadrature points using cubic spline interpolation to reduce the number of single point CCSD(T)-F12a/cc-pVTZ-F12 calculations. In contrast, the  $\mathbf{G}$  matrix elements were not interpolated, but calculated directly at each quadrature point.

## B. Coordinates

The structure of the water dimer can be described by 12 curvilinear internal coordinates, chosen to be  $r_1, r_2, t_a, r_3, r_4, t_d, R, \theta, \phi, \alpha, \beta$ , and  $\gamma$ . The intramolecular coordinates  $\{r_1, r_2, t_a\}$  and  $\{r_3, r_4, t_d\}$  are the bond lengths ( $r$ ) and the bond angles ( $t$ ) of the acceptor and donor units, respectively. As seen in [Fig. 1](#),  $R$  is the distance between the center of masses (CoMs) of the two units. The intermolecular angles  $\phi$  and  $\gamma$  describe the rotation of the acceptor and donor around the bisector of their bond angles, respectively, and  $\theta$  and  $\beta$  denote the angle between these bisectors and the CoM–CoM axis, respectively. The angle  $\alpha$  describes the rotation of the two  $\text{H}_2\text{O}$  units relative to each other along the CoM–CoM axis. In Sec. S2 A of the [supplementary material](#), we provide instructions on how Cartesian coordinates are obtained from the internal coordinates. The values of the internal coordinates corresponding to the equilibrium structure for the different PESs are shown in Table S7. Since the CoM–CoM distance depends on the masses of the atoms, we note here that the masses  $m_{\text{H}} = 1.007\,825 \text{ u}$  and  $m_{\text{O}} = 15.994\,915 \text{ u}$  have been used.

## C. Symmetry aspects

Molecular symmetry (MS) groups<sup>32</sup> can be employed to describe the true (observable) symmetry of vibrational–rotational tunneling (VRT) states of molecules. The MS group includes feasible permutations of identical nuclei and the inversion operator. The MS group of the water dimer is  $G_{16}$  [isomorphic to the  $D_{4h}(M)$  group], which includes permutation of the hydrogens within the

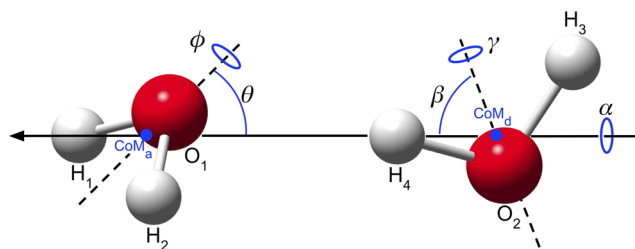


**FIG. 1.** Definition of the intermolecular internal coordinates of the water dimer and the numbering of the atoms of the two  $\text{H}_2\text{O}$  units.

monomers, permutation of the donor and acceptor, and the inversion operation.<sup>32,44</sup> In Table I, we show the effect of the generators of  $G_{16}$ , and its subgroup  $G_8$  (where the permutation of the donor and acceptor units is excluded), on the internal coordinates. Applying the operators of  $G_{16}$  results in 16 different numberings of the nuclei of the water dimer. However, since the equilibrium structure has  $C_s$  point-group symmetry (see Fig. 1), there are only eight distinct versions of the equilibrium structure that can be interconverted into each other. These eight versions are separated by relatively small barriers; therefore, tunneling between the different minima is pronounced, causing each vibrational level to split into eight VRT levels. For further details on employing symmetry for the water dimer, see Refs. 32 and 44.

As the VRT states transform according to the irreducible representations of the MS group(s), it is possible to construct the Hamiltonian matrix in a block-diagonal form, where each block corresponds to one irreducible representation of (a subgroup of) the MS group. This facilitates the assignment of the computed states and improves the convergence properties of the diagonalization routine, as the almost degenerate states are treated independently.

To take advantage of permutation-inversion symmetry, the reference structure and the coordinate choice should be compatible with the generators of the group. This means that the 1D eigenfunctions (or their product) corresponding to the 1D Hamiltonian of Eq. (5) should be eigenfunctions of the permutation-inversion operators as well. Based on this restriction, we use the  $G_8$  MS group<sup>32</sup> to construct the block-diagonal form of the Hamiltonian matrix. For the coordinate definition used in this work, the reference value of OH bond lengths of the donor should be equal as should the OH bond lengths of the acceptor. We define the reference structure of a given PES from the optimized geometry, where the OH bond lengths of the donor are set to the average of the two OH bond lengths (see Table S7 for reference and optimized structures). In this case, the 1D potential along  $\phi$  is symmetric for  $\phi \rightarrow \phi + \pi$  and  $\phi \rightarrow 2\pi - \phi$ ,

and the same is true for  $\gamma$ , and the 1D potential along  $\alpha$  is symmetric for  $\alpha \rightarrow 2\pi - \alpha$ . Therefore, the 1D eigenfunctions for  $\phi$ ,  $\gamma$ , and  $\alpha$  are eigenfunctions of the generators [(12), (34) and  $E^*$ ] of  $G_8$  [see Table I]. For the chosen reference structure, the potential energy surface in the  $\beta$  and  $\theta$  directions is not symmetric around  $\pi/2$ . Therefore, the 1D eigenfunctions for  $\beta$  and  $\theta$  are not eigenfunctions of the  $P_{da}$  operator present in  $G_{16}$ , and primitive basis functions should be used for these two coordinates in order to utilize  $G_{16}$ . As  $P_{da}$  interchanges the donor and acceptor units, and in addition to the constraint on the basis functions associated with the  $\beta$  and  $\theta$  coordinates, both OH-bond lengths and HOH-bond angles of the reference structure should be equivalent to take advantage of  $G_{16}$ . To avoid this constraint, we have opted for using the subgroup  $G_8$ , rather than  $G_{16}$ . Using only  $G_8$  also allows us to use reduced-dimensional models, where the internal coordinates of one monomer are frozen while active for the other monomer. The symmetry adaptation of the OH-stretching basis functions is described in the Appendix.

In order to construct the block-diagonal Hamiltonian, we determine the character of each permutation-inversion operator for a given basis function and compare the result with the character table of  $G_8$  to determine which irreducible representation the given basis function belongs to.<sup>32</sup> Then, we construct the individual blocks of the Hamiltonian matrix from those basis functions that transform as a given irreducible representation. Using the  $G_8$  MS group results in eight blocks, which significantly reduces the cost of the diagonalization.

#### D. Polyad truncation and energy ceiling

In VibMEMIC, two strategies are followed to limit the size of the variational basis: a polyad number truncation and an energy ceiling. The polyad truncation is of the type

$$P = \sum_n^M P_n v_n \leq P_{\max},$$

where  $v_n$  is the  $n$ th quantum number,  $P_n$  is a coefficient, and  $P_{\max}$  is the maximum polyad number. For the three vibrations of  $H_2O$ , one would typically choose  $P_1 = 2$ ,  $P_2 = 1$ , and  $P_3 = 2$  such that the stretch–bend Fermi resonances are included in the basis for each value of the quantum numbers included for the OH stretches. Defining effective polyad truncations is crucial in terms of reducing the computational cost of FBR calculations. The maximum polyad number controls the size of the Hamiltonian, but not the relative size of its blocks. For a given value of  $P_{\max}$ , blocks with basis functions that transform as different irreducible representations can be of different sizes. The states associated with the largest block will be better converged compared to states associated with smaller blocks. The vibrational tunneling states of the water dimer transform as different irreducible representations. An inappropriate value of  $P_{\max}$  can introduce errors in the calculated tunneling splittings if the magnitude of the tunneling splittings is comparable to the convergence of the energy levels. Hence, we use a polyad truncation for the  $\phi$  and  $\gamma$  modes to ensure that the different blocks in the Hamiltonian are of similar size.

Setting an energy ceiling is another way to control the size of the basis ( $E_{v_1 v_2 \dots v_M} \leq E_{\max}$ ). However, as the  $E_{v_1 v_2 \dots v_M}$  energy levels are not known *a priori*, the ceiling is typically based on a sum

**TABLE I.** Action of the generators<sup>3</sup> of the molecular symmetry groups  $G_8$  and  $G_{16}$  on the internal coordinates. See Fig. 1 for the definition of the coordinates.

| $E$      | $G_{16}$     |                |                 | $P_{da}$       |
|----------|--------------|----------------|-----------------|----------------|
|          | $G_8$        |                |                 |                |
|          | (12)         | (34)           | $E^*$           |                |
| $\beta$  | $\beta$      | $\beta$        | $\beta$         | $\pi - \theta$ |
| $\theta$ | $\theta$     | $\theta$       | $\theta$        | $\pi - \beta$  |
| $\phi$   | $\phi + \pi$ | $\phi$         | $2\pi - \phi$   | $\gamma + \pi$ |
| $\alpha$ | $\alpha$     | $\alpha$       | $-\alpha$       | $\alpha$       |
| $\gamma$ | $\gamma$     | $\gamma + \pi$ | $2\pi - \gamma$ | $\phi + \pi$   |
| $r_1$    | $r_2$        | $r_1$          | $r_1$           | $r_3$          |
| $r_2$    | $r_1$        | $r_2$          | $r_2$           | $r_4$          |
| $t_a$    | $t_a$        | $t_a$          | $t_a$           | $t_d$          |
| $r_3$    | $r_3$        | $r_4$          | $r_3$           | $r_1$          |
| $r_4$    | $r_4$        | $r_3$          | $r_4$           | $r_2$          |
| $t_d$    | $t_d$        | $t_d$          | $t_d$           | $t_a$          |

<sup>a</sup>Generator (12) permutes  $H_1$  and  $H_2$ , (34) permutes  $H_3$  and  $H_4$ , and  $E^*$  denotes the inversion. The generator  $P_{da} \equiv (O_1 O_2)(13)(24)$  permutes the donor and acceptor nuclei.

of the 1D energy levels ( $E_{v_1 v_2 \dots v_M} \approx \sum_n^M E_{v_n}^{1D} = E_{v_1 v_2 \dots v_M}^{\text{approximate}} \leq E_{\text{max}}$ ). Again, care must be taken with respect to resolving tunneling splittings that are comparable to the convergence of the energy levels as  $E_{\text{max}}$  also controls the total size of the Hamiltonian, but not the relative size of its blocks. In VibMEMIC, both the maximum polyad number and the energy ceiling are chosen to best address the specific problem, and only basis functions that satisfy both truncations are included. In computations with both intramolecular (high-frequency) and intermolecular (low-frequency) modes, polyad truncations and energy ceilings are defined for each set of modes (see Sec. S1). For the HF dimer, it was recently demonstrated that few intermolecular (compact) basis functions were needed to converge the intramolecular transitions.<sup>45</sup> This illustrates why separate truncations of the intra- and intermolecular modes are effective.

### E. Notation of transitions

In Sec. IV, we present intramolecular transitions calculated with different vibrational models. We only give the final state of the transitions as all arise from the ground state. The final state for the intramolecular acceptor transitions is denoted as  $|v_i v_j; \pm v_k\rangle$ , where  $v_i$  and  $v_j$  refer to the OH stretch quanta and  $v_k$  refers to the HOH bend quanta. The two OH stretches of the donor are not equivalent, and the final states for the intramolecular donor transitions are denoted as  $|v_m)_f |v_n)_b |v_l\rangle$ , where  $v_m$  and  $v_n$  refer to the free (f) and bound (b) OH stretch quanta, respectively, while  $v_l$  refers to the HOH bend quanta.

### III. FBR VS DVR

The so-called fourth-age<sup>46</sup> variational nuclear-motion code GENIUSH,<sup>36–38</sup> based on the discrete variable representation (DVR) of the Hamiltonian,<sup>47–52</sup> was employed extensively to benchmark the FBR-based VibMEMIC code. GENIUSH can be used to solve the time-independent nuclear Schrödinger equation and obtain rovibrational eigenenergies for systems that exhibit several interacting minima. Furthermore, the code allows for the straightforward setup of reduced-dimensional models in arbitrary curvilinear internal coordinates. In GENIUSH, both the kinetic and the potential energy operators are treated “exactly,” that is, no approximations are introduced. The latest version<sup>38</sup> of the GENIUSH code is capable of treating block-diagonal Hamiltonian matrices, formed according to the irreducible representations of the MS group<sup>32</sup> of the molecule, or at least a subgroup of it.

Although GENIUSH is able to treat rotations,<sup>37</sup> here, we only discuss vibrations, for which the Hamiltonian is given in Eq. (1). The basis is the direct product of one-dimensional primitive DVR functions corresponding to each internal coordinate,

$$\psi_{n_1, n_2, \dots, n_M}(q_1, \dots, q_M) = \prod_{k=1}^M \chi_{n_k}(q_k), \quad (9)$$

where  $\chi_{n_k}(q_k)$  is the  $n_k$ th DVR basis function corresponding to the  $q_k$  coordinate. If  $N_1^0, N_2^0, \dots, N_M^0$  primitive DVR functions are used for the first, second,  $\dots$ , and  $M$ th coordinate, the size of the full

direct-product basis is  $N^{\text{tot}} = \prod_{k=1}^M N_k^0$ . The  $N^{\text{tot}} \times N^{\text{tot}}$ -dimensional matrix of the potential energy becomes diagonal in this basis,

$$V_{(n_1, \dots, n_M), (n'_1, \dots, n'_M)} = V(q_{1, n_1}, \dots, q_{M, n_M}) \prod_{k=1}^M \delta_{n_k, n'_k}, \quad (10)$$

where  $q_{k, n_k}$  is the  $n_k$ th DVR quadrature (grid) point corresponding to the  $k$ th coordinate. The representation of the kinetic energy operator is also an  $N^{\text{tot}} \times N^{\text{tot}}$ -dimensional matrix. Therefore, the elements of  $\mathbf{G}$  and  $\tilde{\mathbf{g}}$  are evaluated at all the grid points and the matrices of the differential operators are also constructed in DVR. The resulting  $N^{\text{tot}} \times N^{\text{tot}}$ -dimensional vibrational Hamiltonian matrix is symmetric and sparse. The required eigenvalues are computed using an iterative Lanczos eigensolver.<sup>53</sup> Table S11 specifies the DVR vibrational basis used in the computations.

To test the accuracy of the FBR-based VibMEMIC model, we have performed a set of reduced-dimensional computations with both VibMEMIC and GENIUSH. In Sec. S3, we show several examples, illustrating that the 1D, 2D, and 3D results with VibMEMIC and GENIUSH generally agree to within  $\leq 0.2 \text{ cm}^{-1}$ .

The water dimer has eight equivalent versions of its equilibrium structure. These version are sampled, for example, in 5D calculations with  $\beta$ ,  $\theta$ ,  $\phi$ ,  $\alpha$ , and  $\gamma$ . However, these eight versions are not equivalent within the many-mode expansion of the PES truncated at third order, which is the approximation utilized in VibMEMIC. As a consequence, the energy levels computed with VibMEMIC appear as two sets of four states, rather than one set of eight states (see Table S3). This symmetry breaking for the many-mode expansion also leads to small non-zero elements in the Hamiltonian connecting the different blocks. We set these small non-zero elements to zero in VibMEMIC to preserve the block-diagonal structure of the Hamiltonian. From our reduced-dimensional computations, we estimate that the difference between enforcing and neglecting this symmetry leads to differences in the intramolecular fundamentals of no more than  $0.2 \text{ cm}^{-1}$ .

Both the new FBR-based VibMEMIC code and the DVR-based GENIUSH code have advantages and limitations and are optimal for slightly different situations. The size of the Hamiltonian matrix is much smaller in the FBR-based VibMEMIC code than in the DVR-based GENIUSH code, which allows for inclusion of more vibrational modes. Furthermore, the efficient truncation of the basis, by the polyad numbers and by the energy ceilings, also helps limit the size of the Hamiltonian matrix within VibMEMIC. Thus, compared to GENIUSH, the diagonalization part of the computation is significantly faster with VibMEMIC.

## IV. RESULTS AND DISCUSSION

### A. The kinetic energy in reduced dimensions

In reduced-dimensional (ro)vibrational models with  $M$  active coordinates, the remaining  $3N - M$  coordinates are inactive (constrained), and an effective Hamiltonian that incorporates these constraints must be constructed. The constraints can either be taken into account by removing the rows and columns involving the constrained coordinates in  $\mathbf{G}$  or by removing the corresponding rows and columns in  $\mathbf{g}$ . The latter option results in a constrained  $\mathbf{G}$  after inversion of  $\mathbf{g}$  [see Eqs. (2) and (3)]. If the coordinates are orthogonal, the two approaches are equivalent. However, if the coordinates

are not orthogonal, the two approaches give rise to different effective Hamiltonians and, consequently, different results. In classical mechanics, constraining the coordinates corresponds to  $dq_i/dt = 0$ , where  $i$  is an index of an inactive mode. The  $\mathbf{G}$  matrix obtained from these types of constraints corresponds to removing columns and rows in  $\mathbf{g}$ . In comparison, the reduction in  $\mathbf{G}$  is equivalent to setting  $p_i = 0$ .

In Table II, we present reduced-dimensional (3D) calculations of the fundamental intramolecular transitions of the two water units in the water dimer, where the two monomers have been separated by 20 Å ( $R = 20$  Å). Since the two monomer units are separated by 20 Å, we expect the fundamentals of the donor and the acceptor to be identical. This is, indeed, the case when  $\mathbf{G}$  is reduced. However, the calculated intramolecular transitions presented in Table II clearly depend on whether the constraints are introduced in  $\mathbf{g}$  or  $\mathbf{G}$ . When  $\mathbf{g}$  is reduced, the intramolecular fundamentals of the two units differ significantly for the bend and the antisymmetric stretch. If  $\mathbf{G}$  is reduced, then the resulting  $\mathbf{G}$  matrix is the same as that of the free water molecule (see Sec. S2 B). In the 3D computations for the donor or acceptor units, the  $\mathbf{G}$  matrix does not depend on  $R$ , and the 3D kinetic energy operator is the same if  $R$  is fixed to its equilibrium value or 20 Å. As shown in Table II, for this particular constrained model, reduction in  $\mathbf{g}$  results in an erroneous description of the intramolecular transitions of the two H<sub>2</sub>O units as clearly illustrated in the dissociation limit. Therefore, we employ the reduction in  $\mathbf{G}$  for the rest of this paper.

## B. Choice of the intermolecular distance coordinate (O–O vs CoM–CoM)

For weakly bound dimers, the coordinates associated with the intermolecular modes are typically defined as five Euler angles and one distance, describing the relative orientation and distance between the donor and acceptor units, respectively. The donor–acceptor distance coordinate is typically defined from the CoMs of the two units, for which an analytical expression for the kinetic energy operator has been derived.<sup>54</sup> In both GENIUSH and VibMEMIC, the kinetic energy operator is represented numerically, which facilitates the exploration of alternative coordinate definitions. One alternative intermolecular distance coordinate in the case of the water dimer is the O–O distance, which is often the distance coordinate of choice if one defines the coordinates from a  $Z$  matrix. The CoM–CoM definition is general for bimolecular complexes, but unlike the O–O definition, it is not isotopically invariant.

**TABLE II.** Fundamental intramolecular transitions ( $\tilde{\nu}$ ), in  $\text{cm}^{-1}$ , of the donor (D) and acceptor (A) unit in the water dimer separated by 20 Å. The results are obtained with a 3D vibrational model utilizing the MB-pol potential<sup>20</sup> and the DVR-based code GENIUSH.

| Final state                   | Reduction in $\mathbf{g}$ |                   | Reduction in $\mathbf{G}$ |                   |
|-------------------------------|---------------------------|-------------------|---------------------------|-------------------|
|                               | $\tilde{\nu}$ (D)         | $\tilde{\nu}$ (A) | $\tilde{\nu}$ (D)         | $\tilde{\nu}$ (A) |
| $ 0\rangle 0\rangle 1\rangle$ | 1586.8                    | 1590.6            | 1594.4                    | 1594.4            |
| $ 10\rangle +0\rangle$        | 3656.1                    | 3656.1            | 3656.1                    | 3656.1            |
| $ 10\rangle -0\rangle$        | 3741.8                    | 3748.6            | 3755.0                    | 3755.0            |

**TABLE III.** Wavenumber differences ( $\Delta\tilde{\nu}$ , in  $\text{cm}^{-1}$ ) of the intramolecular fundamentals with and without including the  $R$  mode. Two different definitions of the donor–acceptor distance coordinate are used. Results are shown for both the donor, (D), and acceptor, (A), unit. The results are obtained with the MB-pol PES<sup>20</sup> using GENIUSH.

| Final state   | CoM–CoM                 |                         | O–O                     |                         |
|---|-------------------------|-------------------------|-------------------------|-------------------------|
|   | $\Delta\tilde{\nu}$ (D) | $\Delta\tilde{\nu}$ (A) | $\Delta\tilde{\nu}$ (D) | $\Delta\tilde{\nu}$ (A) |
| $ 0\rangle_f 0\rangle_b 1\rangle$ or $ 00\rangle 1\rangle$  | −0.38                   | 0.07                    | −1.21                   | 0.72                    |
| $ 0\rangle_f 1\rangle_b 0\rangle$ or $ 10\rangle +0\rangle$ | −0.10                   | 0.01                    | 1.21                    | −0.10                   |
| $ 1\rangle_f 0\rangle_b 0\rangle$ or $ 10\rangle -0\rangle$ | 3.41                    | 0.28                    | −4.63                   | 0.31                    |

We define the optimal intermolecular distance coordinate as the one that has the least impact on the intramolecular fundamental transitions. This choice would likely require fewer basis functions to converge the intramolecular fundamental transitions. In Table III, we show the wavenumber shift of the intramolecular fundamentals calculated from a (3 + 1)D and a 3D calculation of the donor and acceptor intramolecular modes. 3D in (3 + 1)D represents the donor or acceptor intramolecular modes, and “+1D” refers to adding the intermolecular mode associated with the distance coordinate, in other words, 4D calculations without an adiabatic separation. The inactive coordinates were fixed to their reference values. As seen in Table III, the CoM–CoM coordinate choice has significantly smaller impact on the intramolecular fundamentals than the O–O choice. Therefore, we employ the CoM–CoM coordinate in all computations.

## C. Interunit coupling

For most practical purposes, the coupling between the intramolecular modes of the donor and acceptor units is expected to be negligible. The addition of such coupling terms to a harmonically coupled anharmonic-oscillator model resulted in transition wavenumber changes of  $\sim 1 \text{ cm}^{-1}$ .<sup>55</sup> In Table IV, we compare selected intramolecular transition wavenumbers calculated with a 3D model for the three intramolecular modes of either the donor or acceptor with those calculated with a 6D model that includes all intramolecular modes simultaneously. As seen in Table IV, the

**TABLE IV.** Calculated transition wavenumbers, in  $\text{cm}^{-1}$ , for selected OH stretch and HOH bend transitions in the water dimer. Results from a 3D model for either the donor or the acceptor modes are compared with the results from the 6D model that includes all six intramolecular modes. The results are obtained using VibMEMIC and the F12 PES.

| Final state                       | 3D     | 6D     | $\Delta\tilde{\nu}$ |
|-----------------------------------|--------|--------|---------------------|
| $ 00\rangle 1\rangle$             | 1596.7 | 1595.2 | −1.5                |
| $ 0\rangle_f 0\rangle_b 1\rangle$ | 1614.2 | 1614.5 | 0.3                 |
| $ 00\rangle 2\rangle$             | 3157.1 | 3155.1 | −2.0                |
| $ 0\rangle_f 0\rangle_b 2\rangle$ | 3191.1 | 3188.7 | −2.4                |
| $ 0\rangle_f 1\rangle_b 0\rangle$ | 3558.0 | 3555.5 | −2.5                |
| $ 10\rangle +0\rangle$            | 3651.7 | 3651.6 | −0.1                |
| $ 1\rangle_f 0\rangle_b 0\rangle$ | 3726.9 | 3726.9 | 0.0                 |
| $ 10\rangle -0\rangle$            | 3746.6 | 3746.0 | −0.6                |

computed intramolecular transition wavenumbers with (6D) and without (3D) interunit coupling (IUC) do not deviate more than  $2.5\text{ cm}^{-1}$ . These transition wavenumber changes are small compared to the shifts induced by the intermolecular modes (*vide infra*). In Secs. IV D and IV E, we focus on the coupling of either the donor or the acceptor intramolecular modes with the intermolecular modes, with the approximation that the interunit coupling can be neglected.

#### D. Coupling between intramolecular and intermolecular modes

In spectra of hydrogen-bonded complexes, the bound XH-stretch fundamental (where X is an electronegative donor atom, for example, O) is often detected, as it typically becomes redshifted, and its intensity is enhanced relative to the corresponding transition of the isolated monomer.<sup>56,57</sup> For complexes with water as the donor unit, the two OH stretches become partly decoupled upon complex formation due to the frequency shift associated with hydrogen-bond formation. The bonded OH stretch,  $\text{OH}_b$ , is redshifted relative to both OH stretches of the monomer because the hydrogen bond weakens the  $\text{OH}_b$  bond. The free OH stretch,  $\text{OH}_f$ , is redshifted relative to the antisymmetric fundamental of the water monomer, as the coupling between the two OH stretches is reduced. In contrast, the bending transitions of the donor unit are blueshifted because the hydrogen bond “locks”  $\text{H}_b$ , which hinders the bending motion.

In order to investigate the effect of the individual intermolecular modes on the OH stretch and HOH bend transitions, we performed a series of (3 + 1)D computations, where the three modes of either the donor or the acceptor unit and one of the intermolecular modes were active. In these computations, symmetry was not utilized. In Fig. 2, we show the shifts of the donor and acceptor fundamentals based on the (3 + 1)D computations relative to 3D computations. The shifts presented in Fig. 2 are obtained with the F12 PES with VibMEMIC, while the results calculated with GENIUSH for the MB-pol and CCpol PESs are given in Sec. IV E. For all computations, the inactive intermolecular coordinates were fixed to their equilibrium values (see Table S7 for the reference structures). Overall, the shifts are similar to previous results obtained with a simplified effective Hamiltonian approach with a similar coordinate system as the one employed here.<sup>22</sup>

For the donor unit, the calculated shifts for the free OH ( $\text{OH}_f$ ) stretch are small, as this oscillator is not directly involved in hydrogen bonding. The shifts induced by coupling to the intermolecular modes can be traced back to either potential or kinetic energy coupling. The small shifts associated with this mode suggest not only that the potential energy coupling with the intermolecular coordinates is small but also that the  $\mathbf{G}$  matrix elements of the intermolecular modes depend only weakly on the OH bond lengths. The shift of the  $\text{OH}_b$  stretch is positive for all coordinates, and it is largest for  $\beta$  and  $\gamma$ . Coupling of  $\beta$  or  $\gamma$  to the donor vibrations enables partially breaking the hydrogen bond,<sup>22,24</sup> thus significantly blueshifting the  $\text{OH}_b$  stretch with respect to the 3D values. A positive displacement of the  $R$  coordinate increases the CoM–CoM distance, partially breaking the hydrogen bond, but negative displacements along this coordinate have the reverse effect. For the water dimer, the net effect of including  $R$  is small, in agreement with what has been found in previous studies.<sup>22,58</sup> For the donor bending fundamental, we observe

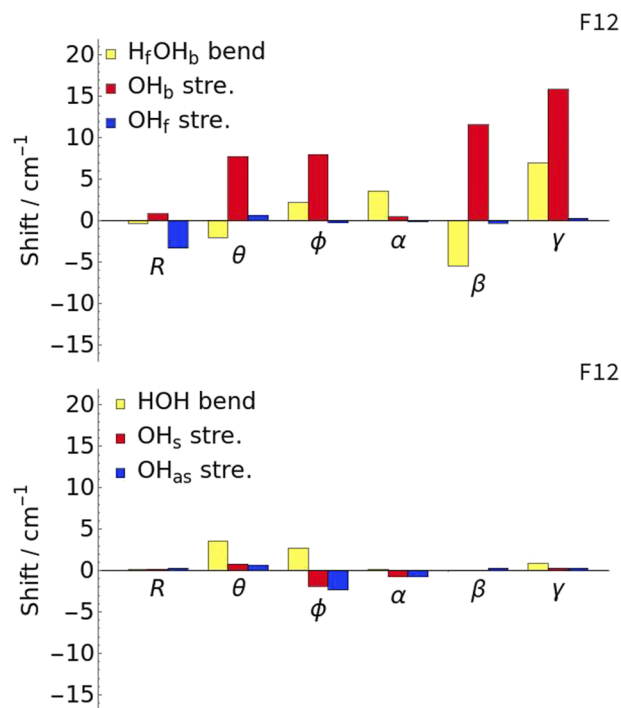


**FIG. 2.** Shifts of the donor (upper panel) and acceptor (lower panel) transitions due to coupling one intermolecular mode [resulting in (3 + 1)D models] to the donor or acceptor intramolecular modes (3D model). The shifts are calculated relative to the 3D results in Table IV. The results were obtained using the F12 PES with VibMEMIC.

negative shifts for  $\theta$  and  $\beta$  and positive shifts for the other angle coordinates, but practically zero shift for  $R$ .

Potential energy coupling is evident when 1D PES cuts along the  $\text{OH}_b$  ( $r_4$ ) or the bending ( $t_d$ ) coordinates depend on the value of the intermolecular coordinates. Kinetic energy coupling is mostly caused by the dependence of  $G_{ij}$  (for the intermolecular angles) on the value of the bond lengths and bond angle. The  $G_{r_4 r_4}$  and  $G_{t_d t_d}$  elements do not depend on the intermolecular angles, and the off-diagonal elements of the  $\mathbf{G}$  matrix have minuscule effect on the vibrations of the donor unit. Cuts of the PES along  $r_4$  and  $t_d$ , corresponding to different values of the intermolecular angles, are shown in Figs. S1 and S2. The  $G_{ii}$  element for  $i = \alpha, \beta, \gamma$ , as a function of  $i$  and  $r_4$  or  $t_d$ , is shown in Fig. S4. In addition, (3 + 1)D computations where all two- and three-mode terms involving the intermolecular mode were excluded from the PES, were used to “turn off” the potential energy coupling (see Table S13). If the results from such computation are similar to the 3D results, then the potential energy coupling is responsible for the shift, while if it is similar to the original (3 + 1)D results, then the shift is due to kinetic energy coupling.

In the case of  $\theta$  and  $\phi$ , the shifts of the donor bend and the  $\text{OH}_b$  stretch modes are fully due to potential energy coupling between the inter- and intramolecular coordinates since the  $\mathbf{G}$  matrix elements involving  $\theta$  and  $\phi$  do not depend on the donor’s intramolecular coordinates and vice versa. This was also confirmed by the fact

that we retrieved the 3D results when we turned off the potential energy coupling in the  $(3 + 1)$ D calculations. In addition, the PES along  $r_4$  or  $t_d$  depends on the value of  $\theta$  and  $\phi$  chosen for the cut, and this dependence mostly explains the direction of the shift. For example, the potential along  $r_4$  becomes steeper if  $\phi$  is not at its equilibrium value, and activating the  $\phi$  coordinate means that these non-equilibrium values are sampled; therefore, the  $\text{OH}_b$  fundamental transition wavenumber increases.

In the case of  $\alpha$ ,  $\beta$ , and  $\gamma$ , both the potential and the kinetic energy coupling may affect the donor bend and the  $\text{OH}_b$  stretch modes. The shift of the donor bend induced by  $\alpha$  and  $\gamma$  is caused mainly by kinetic energy coupling since the PES along  $t_d$  only slightly depends on  $\alpha$  and  $\gamma$ . In contrast,  $G_{\alpha\alpha}$  and  $G_{\gamma\gamma}$  strongly depend on  $t_d$ . The redshift of the bending due to  $\beta$  can be traced to potential energy coupling. This is evident from the  $(3 + 1)$ D calculations with the potential energy coupling turned off. The PES along  $t_d$  becomes less steep if  $\beta$  is not at its equilibrium value, and  $G_{\beta\beta}$  depends only slightly on  $t_d$ . The shift of  $\text{OH}_b$  due to  $\beta$  and  $\gamma$  involves both the kinetic and potential energy coupling. In the case of  $\beta$  and  $\gamma$ , the potential energy coupling causes a large positive shift (in agreement with the 1D PES cuts), while the kinetic energy coupling causes a small negative shift in the case of  $\beta$ . The kinetic energy coupling between  $\gamma$  and the donor turned out to be very sensitive to the OH bond lengths, and consequently, the induced shifts depend on the average bond length, which depend on the PES. For example, in the case of the MB-pol PES, kinetic energy coupling for  $\gamma$  induces  $-3.9$  and  $-0.5$   $\text{cm}^{-1}$  shifts in the  $\text{OH}_b$  and  $\text{OH}_f$  transition wavenumbers, respectively, while the shifts are  $1.2$  and  $-1.9$   $\text{cm}^{-1}$  for the F12 PES.

For the acceptor unit, the wavenumber differences between the  $(3 + 1)$ D and the 3D computations are shown in the lower panel of Fig. 2. The intramolecular fundamentals of the acceptor unit are not strongly affected by complex formation and are similar to those of

an isolated water molecule. The shifts seen for the fundamentals of the acceptor unit are, indeed, much smaller than those seen for the donor unit in the upper panel of Fig. 2. The largest corrections to the bending transition are seen for  $\theta$  and  $\phi$ , the two intermolecular modes directly associated with the acceptor unit. By performing calculations with only kinetic energy or potential energy coupling between the intra- and intermolecular modes, we traced the majority of the effect to a single term in the kinetic energy operator for each intermolecular mode. The diagonal  $\mathbf{G}$  matrix elements for  $\theta$  and  $\phi$ ,  $G_{\theta\theta}$  and  $G_{\phi\phi}$ , respectively, both strongly depend on the HOH bending angle of the acceptor unit. This dependence is far from linear, and the vibrationally averaged kinetic energy of these intermolecular modes is thus different for the HOH-bending ground and excited states, resulting in the observed wavenumber corrections seen in the lower panel of Fig. 2 for the acceptor bending transition.

To investigate whether the shifts from each of the intermolecular modes are additive, we performed 15 sets of  $(3 + 2)$ D model calculations. The “+2D” means adding a pair of intermolecular modes to the 3D model of the intramolecular modes, resulting in a 5D calculation. The shifts calculated with 15 different  $(3 + 2)$ D models for the  $\text{OH}_b$  stretch and HOH bend fundamental of the donor unit are shown in the upper triangles of the two panels of Fig. 3. In the lower triangles of Fig. 3, we show the shifts computed for the  $(3 + 2)$ D models minus the shifts calculated for the related two  $(3 + 1)$ D models. The upper triangles thus display the total shifts calculated with different  $(3 + 2)$ D models, while the lower triangles reflect the degree to which the shifts are additive.

For the donor HOH bend fundamental, the  $(3 + 2)$ D shifts for pairs involving  $\gamma$  are positive, while negative values occur for pairs involving  $\beta$ . This correlates with the  $(3 + 1)$ D results for  $\gamma$  or  $\beta$  (Fig. 2). The largest discrepancies in the additivity of the  $(3 + 1)$ D shifts for the bending are observed for the  $(\theta, \beta)$  and  $(\phi, \beta)$  pairs

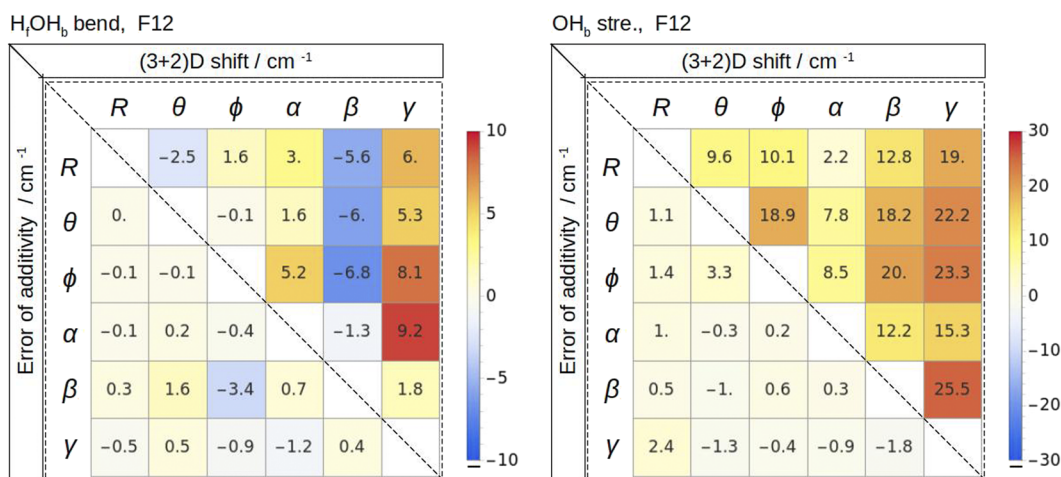


**FIG. 3.** The upper triangles show the shifts of the bend and  $\text{OH}_b$  stretch donor vibrations obtained by coupling two intermolecular modes to the three donor modes [(3 + 2)D model]. The shifts are calculated relative to the 3D results in Table IV. In the lower triangles, the error of additivity is shown and is defined as the difference between the  $(3 + 2)$ D shifts and the two  $(3 + 1)$ D shifts, which involve the two intermolecular modes in the  $(3 + 2)$ D model. For example, the shift of the  $\text{OH}_b$  stretch from coupling to  $\theta$  and  $\phi$  is  $18.9$   $\text{cm}^{-1}$ , but is calculated to be  $15.6$   $\text{cm}^{-1}$  from the corresponding two  $(3 + 1)$ D calculations, resulting in “an error of additivity” of  $3.3$   $\text{cm}^{-1}$ . Note the significant difference in the two color scales. The results were obtained using the F12 PES with VibMEMIC.

[1.6 and  $-3.4\text{ cm}^{-1}$  error in the  $-6.0$  and  $-6.8\text{ cm}^{-1}$  ( $3 + 2$ )D shifts, respectively]. For the bound OH stretch fundamental, the largest discrepancy is found for the  $(\theta, \phi)$  pair, with a  $3.3\text{ cm}^{-1}$  error in the  $18.9\text{ cm}^{-1}$  shift. For most pairs, the ( $3 + 2$ )D corrections are approximated well by the sum of two ( $3 + 1$ )D shifts.

We attribute the partial breakdown of the additivity of the shifts for the bend, but not for the bound OH stretch, to the difference in the nature of the coupling to the intermolecular modes. The PES along the bound OH-stretching coordinate changes significantly upon varying the value of some of the intermolecular coordinates. The intermolecular modes predominantly affect the bound OH stretch due to vibrational averaging effects, and not through resonances between states with excitations in both the bound OH stretch and the intermolecular modes. In contrast, analogous resonances do play an important role for the bending states. The strength of a resonance depends on the size of the coupling element and the energy difference between the states involved in the resonance. When two intermolecular modes are included simultaneously, the two intermolecular modes couple, thus altering the energy levels associated with each intermolecular mode and hence the strength of the resonance(s)—leading to a partial breakdown of the additivity of the shifts for the bend.

In general, the additivity of the calculated shifts works well, which indicates that the total shift induced by all intermolecular modes can be approximated by the sum of the six ( $3 + 1$ )D shifts. The error of this approximation can be estimated by the size of the errors in the additivity found from the ( $3 + 2$ )D calculations. The advantage of replacing a 9D calculation, including three intramolecular and six intermolecular modes, with six 4D calculations is obvious.

### E. Comparison of potential energy surfaces

We have used three different PESs: CCSD(T)-F12a/cc-pVTZ-F12 (abbreviated as F12), CCpol-8sfIR,<sup>19,23</sup> the (CCpol-8sfIR[2012], Radau  $f = 1$  embedding) version from the supplementary material of Ref. 23 (abbreviated as CCpol), and MB-pol.<sup>20</sup> In Table V, we show the OH stretch and HOH bend transition wavenumbers from 3D calculations and from 3D, including the sum of the shifts from the six ( $3 + 1$ )D computations [the ( $3 + \sum 1$ )D model]. We observe that the 3D wavenumbers of the stretching transitions are similar for the F12 and the MB-pol PESs, while the CCpol results are different. For example, the OH<sub>b</sub> stretch

**TABLE V.** Transition wavenumbers, in  $\text{cm}^{-1}$ , for selected intramolecular transitions calculated for different PESs based on either 3D calculations or including the sum of the six calculated ( $3 + 1$ )D shifts, ( $3 + \sum 1$ )D.

| Final state                       | 3D     |        |        | $(3 + \sum 1)$ D |        |        |
|-----------------------------------|--------|--------|--------|------------------|--------|--------|
|                                   | F12    | MB-pol | CCpol  | F12              | MB-pol | CCpol  |
| $ 00\rangle 1\rangle$             | 1596.7 | 1594.4 | 1597.1 | 1603.8           | 1600.6 | 1601.5 |
| $ 0\rangle_f 0\rangle_b 1\rangle$ | 1614.2 | 1607.9 | 1608.8 | 1618.7           | 1614.2 | 1613.3 |
| $ 00\rangle 2\rangle$             | 3157.1 | 3150.9 | 3157.3 | 3172.6           | 3165.2 | 3167.6 |
| $ 0\rangle_f 0\rangle_b 2\rangle$ | 3191.1 | 3177.5 | 3180.6 | 3197.7           | 3188.5 | 3189.6 |
| $ 0\rangle_f 1\rangle_b 0\rangle$ | 3558.0 | 3553.6 | 3543.3 | 3602.1           | 3598.5 | 3585.0 |
| $ 10\rangle_+ 0\rangle$           | 3651.7 | 3654.4 | 3657.3 | 3649.9           | 3649.7 | 3647.5 |
| $ 1\rangle_f 0\rangle_b 0\rangle$ | 3726.9 | 3728.4 | 3738.0 | 3723.4           | 3731.4 | 3734.0 |
| $ 10\rangle_- 0\rangle$           | 3746.6 | 3745.9 | 3750.7 | 3744.6           | 3743.8 | 3738.9 |

fundamental obtained with the CCpol PES is about  $15\text{ cm}^{-1}$  lower than the F12 and MB-pol values, while the OH<sub>f</sub> stretch fundamental is higher by a similar amount. The three PESs also give rise to considerable differences for the donor bend, where there is  $\sim 6\text{ cm}^{-1}$  difference between the F12 and MB-pol values for the fundamental transition.

In Figs. 4 and 5, we show ( $3 + 1$ )D shifts computed with the different PESs for the donor and acceptor OH stretch and HOH bend transitions, respectively. The F12 and the MB-pol PES give very

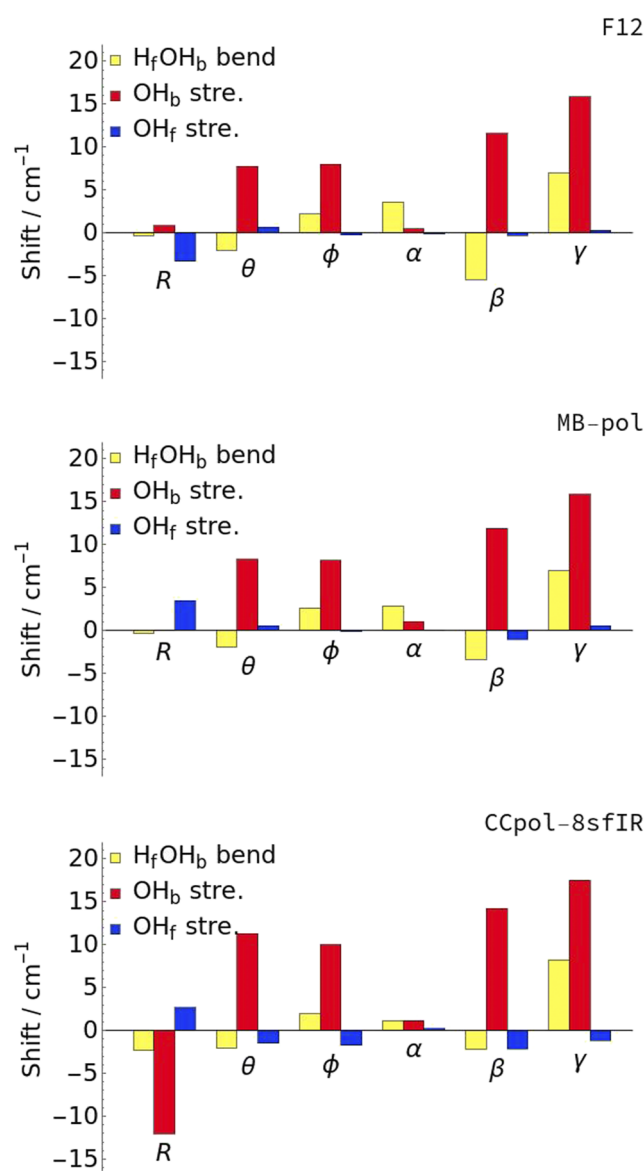


**FIG. 4.** Upper panel: F12 PES, VibMEMIC. Middle panel: MB-pol, GENIUSH. Lower panel: CCpol-8sfIR PES, GENIUSH. Shift of the donor vibration energies due to coupling one intermolecular mode [( $3 + 1$ )D model] to the intramolecular modes of the donor (3D model). The shifts are calculated relative to the 3D results in Table V. Note the different scale with respect to Fig. 5.

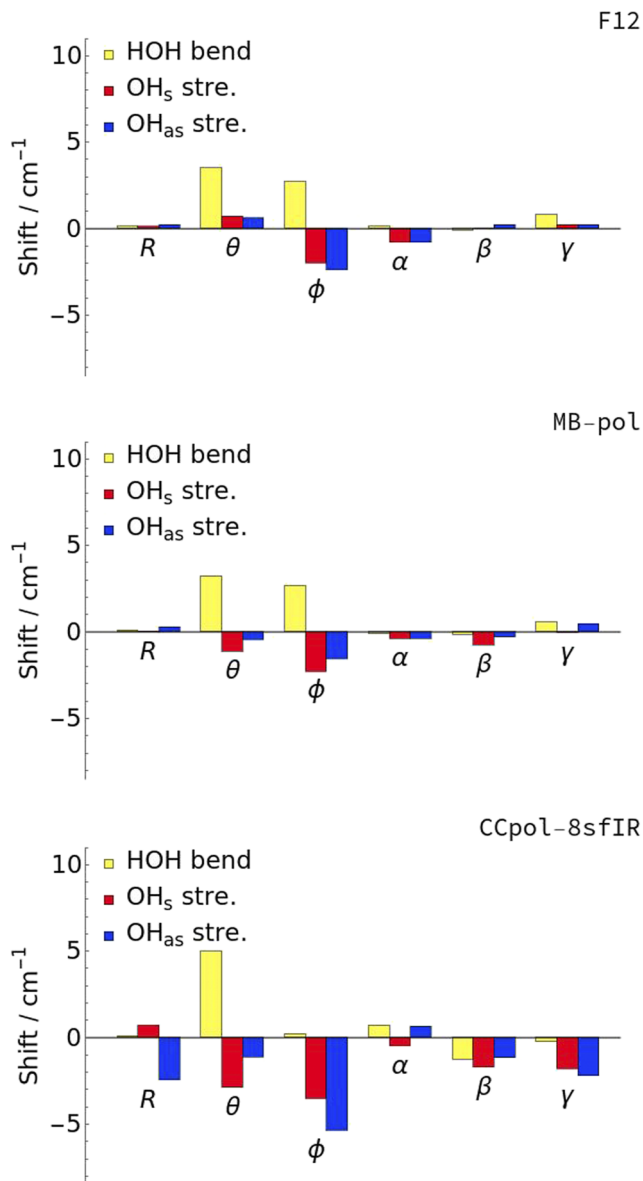


**FIG. 5.** Upper panel: F12 PES, VibMEMIC. Middle panel: MB-pol PES, GENIUSH. Lower panel: CCpol-8sfIR PES, GENIUSH. Shift of the acceptor vibration energies due to coupling one intermolecular mode [(3 + 1)D model] to the internal coordinates of the donor (3D model). The shifts are calculated relative to the 3D results in Table V. Note the different scale with respect to Fig. 4.

similar (3 + 1)D shifts, the most noticeable difference is the difference in sign of the shift of the OH<sub>f</sub> wavenumber due to R. The difference in sign gives rise to the increase in the difference of the OH<sub>f</sub> wavenumbers computed with the MB-pol and F12 PESs from 1.5 cm<sup>-1</sup> in the 3D model to 8.0 cm<sup>-1</sup> in the (3 + ∑1)D model.

The most significant difference between the results with CCpol and the two other PESs is the large negative shift of -12.1 cm<sup>-1</sup> for OH<sub>b</sub> due to R. The OH<sub>b</sub> shifts calculated with CCpol are slightly

larger for the other intermolecular modes. For the F12 and MB-pol PES, the 1D cuts along OH<sub>b</sub> (see Figs. S2 and S3) become less steep if R is decreased and steeper if R is increased. The magnitude of the change is similar for positive and negative displacements of R from the reference value. Furthermore, the 1D ground state wave function for R can to a first approximation be treated as being symmetric with respect to positive and negative displacements, which explains the close to zero total shift of OH<sub>b</sub>. For the CCpol PES, the 1D cuts along OH<sub>b</sub> are similar to those obtained with the other two PESs for increasing R, but become much less steep for negative displacements of R, thus explaining the large redshift of OH<sub>b</sub> due to R seen in Fig. 4. Interestingly, for the OH<sub>b</sub> fundamental transition, the large redshift due to R is partly compensated by the increased blueshift for the other modes in the (3 + ∑1)D model, and the difference between the F12 and the CCpol values is quite similar in the 3D model and the (3 + ∑1)D model (Table V). However, for the CCpol PES, the resulting OH<sub>b</sub> fundamental in the (3 + ∑1)D model is 16 cm<sup>-1</sup> less than the experimental value of 3601 cm<sup>-1</sup> (*vide infra*), while the agreement with experiment is better than 2 cm<sup>-1</sup> for the two other PESs. This suggests that the coupling of OH<sub>b</sub> with R is overestimated in the CCpol PES, which is partly compensated by the overestimation of the coupling with the other coordinates. For the CCpol PES, we find from the (3 + 2)D donor computations that the additivity of the (3 + 1)D shifts breaks down if one of the coordinates is R, while there are no problems for F12 and MB-pol. This again suggests that the coupling with R may not be perfectly described in the CCpol PES.

The calculated (3 + 1)D shifts of the acceptor vibrations are also different for the CCpol PES and the two other PESs. The redshifts of the symmetric and antisymmetric stretches are larger in the case of the CCpol PES. Overall, the results for the F12 surface and the MB-pol PES are very similar for these reduced-dimensional computations, but the CCpol PES gives somewhat different results.

## F. Reduced- vs full-dimensional models

In Table VI, observed and computed wavenumbers are presented for selected OH stretch and HOH bend intramolecular transitions. The observed values are obtained from different jet-expansion experiments.<sup>59–64</sup> The computed values are obtained with different reduced-dimensional vibrational models and with a full 12D vibrational model using VibMEMIC and the F12 PES.

As seen in Table VI, the wavenumbers computed with the 3D model are already within about 6 cm<sup>-1</sup> of the observed values for five of the six fundamentals. The exception is the bound OH-stretch, which is the mode most affected by dimer formation and, as a consequence, also by the intermolecular modes.<sup>22,56</sup> For the bound OH stretch fundamental, the shifts induced by the intermolecular modes were found to be largely additive (see Sec. IV D). Based on the additivity analysis, it is not surprising that the (3 + ∑1)D model significantly improves the OH<sub>b</sub> fundamental transition wavenumber. The 3D calculated OH<sub>b</sub> fundamental transition wavenumber is 43 cm<sup>-1</sup> from the observed value, but improves to within ~1 cm<sup>-1</sup> of the observed value with the (3 + ∑1)D model.

For the other intramolecular fundamentals, the calculated differences between the 3D and (3 + ∑1)D results are less than 7 cm<sup>-1</sup>, and the agreement with the experimental values remains good. The interunit coupling is small (Sec. IV C), and adding the calculated

**TABLE VI.** Transition wavenumbers, in  $\text{cm}^{-1}$ , for selected intramolecular transitions of the two water units in the water dimer calculated with different vibrational models. The calculated results were obtained using the F12 PES with VibMEMIC. The convergence of the 9D and 12D results is shown in Sec. S1.

| Final state                       | 3D     | $(3 + \sum 1)\text{D}$ | $(3 + \sum 1)\text{D}+\text{IUC}$ | 9D     | 9D+IUC | 12D    | Jet                  |
|-----------------------------------|--------|------------------------|-----------------------------------|--------|--------|--------|----------------------|
| $ 00\rangle 1\rangle$             | 1596.7 | 1603.8                 | 1602.3                            | 1605.8 | 1604.3 | 1605.5 | 1600.6 <sup>61</sup> |
| $ 0\rangle_f 0\rangle_b 1\rangle$ | 1614.2 | 1618.7                 | 1619.0                            | 1616.6 | 1616.9 | 1616.7 | 1620 <sup>61</sup>   |
| $ 00\rangle 2\rangle$             | 3157.1 | 3172.6                 | 3170.6                            | 3178.0 | 3176.0 | 3177.2 | ...                  |
| $ 0\rangle_f 0\rangle_b 2\rangle$ | 3191.1 | 3197.7                 | 3195.3                            | 3194.9 | 3192.5 | 3198.8 | ...                  |
| $ 0\rangle_f 1\rangle_b 0\rangle$ | 3558.0 | 3602.1                 | 3599.6                            | 3600.0 | 3597.5 | 3597.5 | 3601 <sup>60</sup>   |
| $ 10\rangle_+ 0\rangle$           | 3651.7 | 3649.9                 | 3649.8                            | 3648.1 | 3648.0 | 3648.2 | 3651 <sup>64</sup>   |
| $ 1\rangle_f 0\rangle_b 0\rangle$ | 3726.9 | 3723.4                 | 3723.4                            | 3721.9 | 3721.9 | 3723.0 | 3730 <sup>59</sup>   |
| $ 10\rangle_- 0\rangle$           | 3746.6 | 3744.6                 | 3744.0                            | 3744.2 | 3743.6 | 3740.7 | 3745.5 <sup>59</sup> |

corrections to the  $(3 + \sum 1)\text{D}$  results slightly improves the agreement of the two bending fundamental transitions and has little impact on the stretching transitions.

The transition wavenumbers calculated with the 9D models, where we include the three intramolecular modes of one  $\text{H}_2\text{O}$  unit and all six intermolecular modes, are similar to those computed with the computationally inexpensive  $(3 + \sum 1)\text{D}$  model. The  $(3 + \sum 1)\text{D}$  and 9D fundamental transitions are within about  $2 \text{ cm}^{-1}$ .

The transition wavenumbers calculated with the 12D model are similar to the results calculated with the 9D and  $(3 + \sum 1)\text{D}$  models. The error arising from the inaccuracy of the electronic structure method is expected to be about  $5 \text{ cm}^{-1}$  with CCSD(T)-F12a/cc-pVTZ-F12.<sup>65–67</sup> The estimated convergence error of the 12D calculations is less than  $2 \text{ cm}^{-1}$  (Table S6). All models give results in excellent agreement with the experimentally observed transitions from jet-expansion experiments. The largest difference between the 12D vibrational calculations and the observed values is seen for the  $\text{OH}_f$  stretch fundamental transition, i.e., also the transition with the largest difference in the  $(3 + 1)\text{D}$  shifts computed with the MB-pol PES and the F12 PES (Sec. IV E).

Even in recent years, the assignment of the  $\text{OH}_b$  stretch fundamental transition in the water dimer has been debated.<sup>34</sup> In jet expansion experiments, both dimers and higher-order (trimer, tetramer, etc.) clusters often contribute to the observed spectra. In our 3D calculations, the  $\text{OH}_b$  stretch fundamental transition is located at  $3558 \text{ cm}^{-1}$ , which happens to be close to the observed  $\text{OH}_b$  stretch fundamental transition of the water trimer. However, including the coupling to the intermolecular modes, the  $\text{OH}_b$  stretch transition of the water dimer blueshifts to about  $3600 \text{ cm}^{-1}$ , as seen from the  $(3 + \sum 1)\text{D}$ , the 9D, and the 12D models. The agreement of these vibrational models suggests that the 12D values are reliable, and the calculated  $\text{OH}_b$  fundamental transition is indeed in excellent agreement with the transition observed at  $3601 \text{ cm}^{-1}$ .<sup>60</sup>

## V. CONCLUSIONS

A new vibrational model and an associated computer code have been developed. The model is based on the finite-basis representation (FBR) of a Hamiltonian expressed in internal coordinates and employs a low-order many-mode expansion of both the kinetic energy operator and the potential energy surface (PES). The

truncations are needed to make the computations on many-mode systems feasible. We use polyad truncations and energy ceilings to control the size of the variational basis. In addition, permutation-inversion symmetry is used to obtain a block-diagonal Hamiltonian, further reducing the cost of the computations. The FBR-based VibMEMIC code developed is applicable to all molecular systems described with either user-defined internal coordinates or internal coordinates based on a  $Z$  matrix. While the code is general in this sense, the polyad truncation, the energy ceiling, and the use of symmetry need to be manually defined for the system of interest.

The VibMEMIC results were benchmarked against a nuclear-motion code, GENIUSH, in which neither the kinetic energy nor the PES operator is approximated. For the OH stretch and HOH bend transitions in the water dimer, we find that the errors resulting from truncations in the VibMEMIC model appear to be less than the intrinsic inaccuracy of the PESs employed. The truncation of the many-mode expansion of the PES leads to a breakdown of the permutation-inversion symmetry ( $G_8$ ) of the Hamiltonian, which primarily affects the tunneling-splitting pattern. Most importantly, the approximations applied in VibMEMIC significantly reduce its computational cost when compared with more exact vibrational models and, as illustrated, facilitate computations with the full 12 vibrational modes of the water dimer.

We have performed a set of computationally inexpensive reduced-dimensional computations with both the FBR- and DVR-based models to understand the applicability of reduced-dimensional effective Hamiltonian approaches. These were designed to investigate how the high-frequency intramolecular transitions are affected by their coupling to the low-frequency intermolecular modes. Not surprisingly, the effects are largest for the OH stretch directly involved in the hydrogen bond. For this mode, the wavenumber shifts from each of the six intermolecular modes were found to be largely additive. The difference between the calculated and experimental transition wavenumber for the bound OH stretch fundamental is improved from  $\sim 43 \text{ cm}^{-1}$  in the 3D calculations to only  $\sim 1 \text{ cm}^{-1}$  upon combining the shifts obtained from six  $(3 + 1)\text{D}$  calculations. The same reduced-dimensional models provide valuable physical insight into the origin of the observable shifts, which may be used to predict intramolecular transition wavenumbers of related molecules and to guide the construction of effective vibrational models.

The 12D results, augmented with the additivity analysis, indicate that the excellent agreement between the observed and the computed transitions is not due to error cancellation. We show that this excellent agreement can be achieved even with the use of reduced-dimensional vibrational models. The accurate calculations of intramolecular transition wavenumber are the first step in obtaining reliable calculated water dimer vibrational spectra.

## SUPPLEMENTARY MATERIAL

See the [supplementary material](#) for additional details on both the VibMEMIC and GENIUSH calculations, benchmarking of the VibMEMIC code, a technical definition of the water dimer coordinate system, a detailed description of why the reduction in  $\mathbf{g}$  leads to an erroneous description of the intramolecular transitions in the presented 3D model of the donor and acceptor unit, converge tests, and additional tables and figures related to the presented results.

## ACKNOWLEDGMENTS

The authors acknowledge funding from NKFH (Grant No. K138233), Independent Research Fund Denmark (Grant No. 9040-00142B), and the Novo Nordisk Foundation Interdisciplinary Synergy Program (Grant No. NNF19OC0057374) and computer time from the High Performance Center at the Faculty of Science at the University of Copenhagen. I.S. was supported by a grant from the ÚNKP-21-3 New National Excellence Programs of the Ministry for Innovation and Technology, supported by the National Research, Development and Innovation Fund.

## AUTHOR DECLARATIONS

### Conflict of Interest

The authors have no conflicts to disclose.

## DATA AVAILABILITY

The data that support the findings of this study are available within the article and its [supplementary material](#). The CCSD(T)-F12a/cc-pVTZ-F12 potential energy surface is available online at <https://erda.ku.dk/archives/58d1c61242c063781b7161c78f0d94e0/published-archive.html>.

## APPENDIX: DETAILS OF VibMEMIC

In Subsection 1 of the [Appendix](#), a detailed description of the formulation of the 1D Hamiltonians, the basis functions, and the choice of quadrature is given. In Subsection 2 of the [Appendix](#), we describe symmetry adaptation of the OH-stretch basis functions.

### 1. 1D Hamiltonians

In Eqs. (4) and (5), the rotational and translational part of the determinant of the Jacobian can be excluded as the  $\hat{p}_i$  (and  $\hat{p}_j$ ) operator only operates on the vibrational coordinates. The vibrational part of the absolute value of the determinant of the Jacobian can be

expressed as  $|\bar{J}_{\text{vib}}| = \prod_{k=1}^{N-1} r_k^2 \prod_{l=1}^{N-2} \sin(\theta_l)$ , where  $r$  is a bond length and  $\theta$  is an angle between 0 and  $\pi$ .<sup>68</sup>

The Jacobian does not depend on angles with a 0 to  $2\pi$  range. The 1D Hamiltonian for these angles is

$$\hat{h}_i = \frac{1}{2} \hat{p}_i^\dagger G_{ii} \hat{p}_i + V_i^{(1D)}(q_i), \quad (\text{A1})$$

where we use a basis set of sine and cosine functions ( $\{\chi(q_i)\}$ ) =  $\{(2\pi)^{-1/2}, \pi^{-1/2} \cos(q_i \cdot n), \pi^{-1/2} \sin(q_i \cdot n)\}$ , with  $n = 1, 2, \dots$ ) and define the derivatives of these functions with respect to the coordinate as  $\chi'_l(q_i) \equiv \frac{\partial \chi_l(q_i)}{\partial q_i}$ .

For angles with a 0 to  $\pi$  range, the 1D Hamiltonian is

$$\hat{h}_i = \frac{1}{2} \sin^{-1/2}(q_i) \hat{p}_i^\dagger G_{ii} \hat{p}_i \sin^{-1/2}(q_i) + V_i^{(1D)}(q_i), \quad (\text{A2})$$

where we use a basis set of associated Legendre polynomials ( $P_l^m(z)$  with  $m = 0$ ), parameterized in terms of  $z = \cos(q_i)$ . Matrix elements of this Hamiltonian are now expressed as

$$\begin{aligned} \langle k|h_i|l \rangle &= \frac{-\hbar^2}{2} \int_0^\pi \chi'_k(q_i) G_{ii} \chi'_l(q_i) dq_i \\ &+ \int_0^\pi \chi_k(q_i) V_i^{(1D)}(q_i) \chi_l(q_i) dq_i, \end{aligned} \quad (\text{A3})$$

where  $\chi_l(q_i) = N_l \sin^{1/2}(q_i) P_l^0(\cos(q_i))$ , with the normalization constant  $N_l = (l + \frac{1}{2})^{1/2}$ , and we define

$$\begin{aligned} \chi'_l(q_i) &\equiv N_l \sin^{1/2}(q_i) \frac{\partial P_l^0(\cos(q_i))}{\partial q_i} \\ &= \frac{N_l \cdot l}{\sin^{1/2}(q_i)} \cdot [\cos(q_i) \cdot P_l^0(\cos(q_i)) - P_{l-1}^0(\cos(q_i))]. \end{aligned} \quad (\text{A4})$$

Note that for angles with a 0 to  $\pi$  range, the  $\chi'_l(q_i)$  functions are not the derivative of the  $\chi_l(q_i)$  functions with respect to the coordinate as they were defined for angles with a 0 to  $2\pi$  range. However, the  $\chi'_l(q_i)$  functions are chosen to satisfy Eq. (A3) with the appropriate limits of integration. The associated Legendre polynomials are orthogonal with respect to the volume element of integration,  $d\tau = \sin(q_i) dq_i$ , thus making the  $\chi_l(q_i)$  functions orthonormal with respect to the volume element of integration,  $d\tau = dq_i$ ,

$$\begin{aligned} \int_0^\pi \chi_k(q_i) \chi_l(q_i) dq_i \\ = N_k N_l \int_0^\pi P_k^0(\cos(q_i)) P_l^0(\cos(q_i)) \sin(q_i) dq_i = \delta_{kl}. \end{aligned} \quad (\text{A5})$$

Associated Legendre polynomials with  $m = 0$  are also used to solve the 1D Schrödinger equation for the stretches, analogous to what have just been shown for angles with a 0 to  $\pi$  range, but with  $q_i \rightarrow (q_i - \min(q_i)) \frac{\pi}{\max(q_i) - \min(q_i)}$ .

For stretches and bends, we use Gauss–Legendre quadrature, and for angles with a 0 to  $2\pi$  range, we use Clenshaw–Curtis quadrature, both with a total of 101 points. In Table S1, we show the displacement ranges used for each internal coordinate. We store the 1D eigenfunctions,

$$\psi_v(q_i) = \sum_l c_{vl} \chi_l(q_i), \quad (\text{A6})$$

where  $c_{vl}$  is the  $l$ th coefficient of the  $v$ th eigenfunctions obtained from diagonalizing the 1D Hamiltonian and also the functions

$$\psi'_v(q_i) = \sum_l c_{vl} \chi'_l(q_i). \quad (\text{A7})$$

Evaluating elements of the  $M$ -dimensional kinetic energy operator with the  $\psi'_v(q_i)$  functions has the advantage of removing the  $\tilde{J}$  terms in the Podolsky Hamiltonian. The functions in Eqs. (A6) and (A7) simplify the kinetic-energy matrix elements,

$$\begin{aligned} & \int_{q_i^{\min}}^{q_i^{\max}} \int_{q_j^{\min}}^{q_j^{\max}} \psi_v(q_i) \psi_u(q_j) T_{ij} \psi_{v'}(q_i) \psi_{u'}(q_j) dq_i dq_j \\ &= \frac{-\hbar^2}{2} \int_{q_i^{\min}}^{q_i^{\max}} \int_{q_j^{\min}}^{q_j^{\max}} \psi'_v(q_i) \psi_u(q_j) G_{ij} \psi_{v'}(q_i) \psi_{u'}(q_j) dq_i dq_j, \end{aligned} \quad (\text{A8})$$

where  $T_{ij} = \frac{1}{2} \tilde{J}^{-1/2} \hat{p}_i^\dagger G_{ij} \tilde{J} \hat{p}_j \tilde{J}^{-1/2}$  and  $q_i^{\min}$  and  $q_i^{\max}$  are the minimal and maximal values of the  $q_i$  coordinate. Equation (A8) can be verified from the definitions of  $\psi'_v(q_i)$ ,  $\chi'_l(q_i)$ , and  $\tilde{J}_{\text{vib}}$ , all of which have known analytical expressions.

## 2. Symmetry adaptation of basis functions

Generators (12) and (34) interchange the OH bonds of the acceptor and the donor units, respectively (see Table I). The two acceptor OH stretches are equivalent, and we chose their basis functions as the 1D eigenfunctions. The product of the acceptor basis functions is, indeed, eigenfunctions of generator (12) if the associated quantum numbers are equivalent,

$$(12)\psi_v(r_1)\psi_v(r_2) = \psi_v(r_2)\psi_v(r_1) = 1 \cdot \psi_v(r_1)\psi_v(r_2). \quad (\text{A9})$$

The two donor OH stretches are not equivalent. However, the basis functions for both the OH<sub>f</sub> stretch and for the OH<sub>b</sub> stretch are chosen as the 1D eigenfunctions of the OH<sub>f</sub> stretch. With this choice, the product of the donor basis functions becomes eigenfunctions of generator (34) if the associated quantum numbers are equivalent.

If the quantum numbers are different ( $v \neq v'$ ), products of the 1D basis functions are not eigenfunctions of the generators,

$$(12)\psi_v(r_1)\psi_{v'}(r_2) = \psi_v(r_2)\psi_{v'}(r_1) \neq \lambda \cdot \psi_v(r_1)\psi_{v'}(r_2), \quad (\text{A10})$$

where  $\lambda$  is a constant. There are two apparent solutions to this challenge, either changing the coordinates to symmetric/antisymmetric displacements of the OH bond lengths from their equilibrium values or using a linear combination of the 1D eigenfunctions as basis functions. We have chosen the latter strategy, resulting in basis functions of the type

$$\psi_{vv\pm}(r_1, r_2) = \frac{1}{\sqrt{2}} (\psi_v(r_1)\psi_{v'}(r_2) \pm \psi_{v'}(r_1)\psi_v(r_2)) \quad (\text{A11})$$

for both the donor and the acceptor OH stretches. The full (12D) basis functions thus take the following form (with the label of the quantum numbers excluded for ease of notation):

$$\begin{aligned} & \Psi(r_1, r_2, t_a, r_3, r_4, t_d, R, \beta, \theta, \phi, \alpha, \gamma) \\ &= \psi(r_1, r_2) \psi(t_a) \psi(r_3, r_4) \psi(t_d) \psi(R) \psi(\beta) \psi(\theta) \psi(\phi) \psi(\alpha) \psi(\gamma). \end{aligned} \quad (\text{A12})$$

## REFERENCES

- M. Van Thiel, E. D. Becker, and G. C. Pimentel, "Infrared studies of hydrogen bonding of water by the matrix isolation technique," *J. Chem. Phys.* **27**, 486–490 (1957).
- T. R. Dyke, K. M. Mack, and J. S. Muentzer, "The structure of water dimer from molecular beam electric resonance spectroscopy," *J. Chem. Phys.* **66**, 498–510 (1977).
- L. B. Braly, J. D. Cruzan, K. Liu, R. S. Fellers, and R. J. Saykally, "Terahertz laser spectroscopy of the water dimer intermolecular vibrations. I. (D<sub>2</sub>O)<sub>2</sub>," *J. Chem. Phys.* **112**, 10293–10313 (2000).
- S. Kassi, P. Macko, O. Naumenko, and A. Campargue, "The absorption spectrum of water near 750 nm by CW-CRDS: Contribution to the search of water dimer absorption," *Phys. Chem. Chem. Phys.* **7**, 2460–2467 (2005).
- T. Kumagai, M. Kaizu, S. Hatta, H. Okuyama, T. Aruga, I. Hamada, and Y. Morikawa, "Direct observation of hydrogen-bond exchange within a single water dimer," *Phys. Rev. Lett.* **100**, 166101 (2008).
- M. Y. Tretyakov, E. A. Serov, M. A. Koshelev, V. V. Parshin, and A. F. Krupnov, "Water dimer rotationally resolved millimeter-wave spectrum observation at room temperature," *Phys. Rev. Lett.* **110**, 093001 (2013).
- E. A. Serov, M. A. Koshelev, T. A. Odintsova, V. V. Parshin, and M. Y. Tretyakov, "Rotationally resolved water dimer spectra in atmospheric air and pure water vapour in the 188–258 GHz range," *Phys. Chem. Chem. Phys.* **16**, 26221–26233 (2014).
- A. Mukhopadhyay, W. T. S. Cole, and R. J. Saykally, "The water dimer. I. Experimental characterization," *Chem. Phys. Lett.* **633**, 13–26 (2015).
- R. Schwan, C. Qu, D. Mani, N. Pal, L. Meer, B. Redlich, C. Leforestier, J. M. Bowman, G. Schwaab, and M. Havenith, "Observation of the low-frequency spectrum of the water dimer as a sensitive test of the water dimer potential and dipole moment surfaces," *Angew. Chem., Int. Ed.* **58**, 13119–13126 (2019).
- K. Morokuma and L. Pedersen, "Molecular-orbital studies of hydrogen bonds. An *ab initio* calculation for dimeric H<sub>2</sub>O," *J. Chem. Phys.* **48**, 3275 (1967).
- D. F. Coker and R. O. Watts, "Structure and vibrational spectroscopy of the water dimer using quantum simulation," *J. Phys. Chem.* **91**, 2513–2518 (1987).
- N. Goldman, R. S. Fellers, M. G. Brown, L. B. Braly, C. J. Keoshian, C. Leforestier, and R. J. Saykally, "Spectroscopic determination of the water dimer intermolecular potential-energy surface," *J. Chem. Phys.* **116**, 10148–10163 (2002).
- D. P. Schofield and H. G. Kjaergaard, "Calculated OH-stretching and HOH-bending vibrational transitions in the water dimer," *Phys. Chem. Chem. Phys.* **5**, 3100–3105 (2003).
- Y. Scribano, N. Goldman, R. J. Saykally, and C. Leforestier, "Water dimers in the atmosphere. III. Equilibrium constant from a flexible potential," *J. Phys. Chem. A* **110**, 5411–5419 (2006).
- D. P. Schofield, J. R. Lane, and H. G. Kjaergaard, "Hydrogen bonded OH-stretching vibration in the water dimer," *J. Phys. Chem. A* **111**, 567–572 (2007).
- X. Huang, B. J. Braams, J. M. Bowman, R. E. A. Kelly, J. Tennyson, G. C. Groenenboom, and A. van der Avoird, "New *ab initio* potential energy surface and the vibration-rotation-tunneling levels of (H<sub>2</sub>O)<sub>2</sub> and (D<sub>2</sub>O)<sub>2</sub>," *J. Chem. Phys.* **128**, 034312 (2008).
- A. Shank, Y. Wang, A. Kaledin, B. J. Braams, and J. M. Bowman, "Accurate *ab initio* and 'hybrid' potential energy surfaces, intramolecular vibrational energies, and classical IR spectrum of the water dimer," *J. Chem. Phys.* **130**, 144314 (2009).
- Y. Wang, X. Huang, B. C. Shepler, B. J. Braams, and J. M. Bowman, "Flexible, *ab initio* potential, and dipole moment surfaces for water. I. Tests and applications for clusters up to the 22-mer," *J. Chem. Phys.* **134**, 094509 (2011).
- C. Leforestier, K. Szalewicz, and A. van der Avoird, "Spectra of water dimer from a new *ab initio* potential with flexible monomers," *J. Chem. Phys.* **137**, 014305 (2012).

- <sup>20</sup>V. Babin, C. Leforestier, and F. Paesani, "Development of a 'first principles' water potential with flexible monomers: Dimer potential energy surface, VRT spectrum, and second virial coefficient," *J. Chem. Theory Comput.* **9**, 5395–5403 (2013).
- <sup>21</sup>J. C. Howard, J. L. Gray, A. J. Hardwick, L. T. Nguyen, and G. S. Tschumper, "Getting down to the fundamentals of hydrogen bonding: Anharmonic vibrational frequencies of (HF)<sub>2</sub> and (H<sub>2</sub>O)<sub>2</sub> from *ab initio* electronic structure computations," *J. Chem. Theory Comput.* **10**, 5426–5435 (2014).
- <sup>22</sup>K. Mackeprang, H. G. Kjaergaard, T. Salmi, V. Hänninen, and L. Halonen, "The effect of large amplitude motions on the transition frequency redshift in hydrogen bonded complexes: A physical picture," *J. Chem. Phys.* **140**, 184309 (2014).
- <sup>23</sup>P. Jankowski, G. Murdachaw, R. Bukowski, O. Akin-Ojo, C. Leforestier, and K. Szalewicz, "Ab *initio* water pair potential with flexible monomers," *J. Phys. Chem. A* **119**, 2940–2964 (2015).
- <sup>24</sup>K. Mackeprang, V. Hänninen, L. Halonen, and H. G. Kjaergaard, "The effect of large amplitude motions on the vibrational intensities in hydrogen bonded complexes," *J. Chem. Phys.* **142**, 094304 (2015).
- <sup>25</sup>A. Mukhopadhyay, S. S. Xantheas, and R. J. Saykally, "The water dimer. II. Theoretical investigations," *Chem. Phys. Lett.* **700**, 163–175 (2018).
- <sup>26</sup>C. L. Vaillant, D. J. Wales, and S. C. Althorpe, "Tunneling splittings from path-integral molecular dynamics using a Langevin thermostat," *J. Chem. Phys.* **148**, 234102 (2018).
- <sup>27</sup>X.-G. Wang and T. Carrington, "Using monomer vibrational wavefunctions to compute numerically exact (12D) rovibrational levels of water dimer," *J. Chem. Phys.* **148**, 074108 (2018).
- <sup>28</sup>M. P. Metz, K. Szalewicz, J. Sarka, R. Tóbiás, A. G. Császár, and E. Mátyus, "Molecular dimers of methane clathrates: *Ab initio* potential energy surfaces and variational vibrational states," *Phys. Chem. Chem. Phys.* **21**, 13504–13525 (2019).
- <sup>29</sup>A. Nandi, C. Qu, P. L. Houston, R. Conte, Q. Yu, and J. M. Bowman, "A CCSD(T)-based 4-body potential for water," *J. Phys. Chem. Lett.* **12**, 10318–10324 (2021).
- <sup>30</sup>L. Pauling, *The Nature of the Chemical Bond* (Cornwall University Press, New York, 1939).
- <sup>31</sup>H. C. Longuet-Higgins, "The symmetry groups of non-rigid molecules," *Mol. Phys.* **6**, 445–460 (1963).
- <sup>32</sup>P. R. Bunker and P. Jensen, *Molecular Symmetry and Spectroscopy* (NRC Research Press, Ottawa, 2006).
- <sup>33</sup>G. R. Low and H. G. Kjaergaard, "Calculation of OH-stretching band intensities of the water dimer and trimer," *J. Chem. Phys.* **110**(18), 9104–9115 (1999).
- <sup>34</sup>E. Vogt and H. G. Kjaergaard, "Vibrational spectroscopy of the water dimer at jet-cooled and atmospheric temperatures," *Annu. Rev. Phys. Chem.* **73**, 209–231 (2022).
- <sup>35</sup>E. Sälli, T. Salmi, and L. Halonen, "Computational high-frequency overtone spectra of the water–ammonia complex," *J. Phys. Chem. A* **115**, 11594–11605 (2011).
- <sup>36</sup>E. Mátyus, G. Czakó, and A. G. Császár, "Toward black-box-type full- and reduced-dimensional variational (ro)vibrational computations," *J. Chem. Phys.* **130**, 134112 (2009).
- <sup>37</sup>C. Fábri, E. Mátyus, and A. G. Császár, "Rotating full- and reduced-dimensional quantum chemical models of molecules," *J. Chem. Phys.* **134**, 074105 (2011).
- <sup>38</sup>C. Fábri, M. Quack, and A. G. Császár, "On the use of nonrigid-molecular symmetry in nuclear-motion computations employing a discrete variable representation: A case study of the bending energy levels of CH<sub>3</sub><sup>+</sup>," *J. Chem. Phys.* **147**, 134101 (2017).
- <sup>39</sup>B. Podolsky, "Quantum-mechanically correct form of Hamiltonian function for conservative systems," *Phys. Rev.* **32**, 812–816 (1928).
- <sup>40</sup>E. B. Wilson, Jr., J. C. Decius, and P. C. Cross, *Molecular Vibrations: The Theory of Infrared and Raman Vibrational Spectra* (McGraw-Hill, New York, 1955).
- <sup>41</sup>T. B. Adler, G. Knizia, and H.-J. Werner, "A simple and efficient CCSD(T)-F12 approximation," *J. Chem. Phys.* **127**, 221106 (2007).
- <sup>42</sup>K. A. Peterson, T. B. Adler, and H.-J. Werner, "Systematically convergent basis sets for explicitly correlated wavefunctions: The atoms H, He, B–Ne, and Al–Ar," *J. Chem. Phys.* **128**, 084102 (2008).
- <sup>43</sup>H.-J. Werner, P. J. Knowles, F. R. Manby, J. A. Black, K. Doll, A. Heßelmann, D. Kats, A. Köhn, T. Korona, D. A. Kreplin, Q. Ma, T. F. Miller, A. Mitrushchenkov, K. A. Peterson, I. Polyak, G. Rauhut, and M. Sibaev, "The Molpro quantum chemistry package," *J. Chem. Phys.* **152**, 144107 (2020).
- <sup>44</sup>T. R. Dyke, "Group theoretical classification of the tunneling–rotational energy levels of water dimer," *J. Chem. Phys.* **66**, 492–497 (1977).
- <sup>45</sup>P. M. Felker and Z. Bačić, "Weakly bound molecular dimers: Intramolecular vibrational fundamentals, overtones, and tunneling splittings from full-dimensional quantum calculations using compact contracted bases of intramolecular and low-energy rigid-monomer intermolecular eigenstates," *J. Chem. Phys.* **151**(2), 024305 (2019).
- <sup>46</sup>A. G. Császár, C. Fábri, T. Szidarovszky, E. Mátyus, T. Furtenbacher, and G. Czakó, "The fourth age of quantum chemistry: Molecules in motion," *Phys. Chem. Chem. Phys.* **14**, 1085–1106 (2012).
- <sup>47</sup>D. O. Harris, G. G. Engerholm, and W. D. Gwinn, "Calculation of matrix elements for one-dimensional quantum-mechanical problems and the application to anharmonic oscillators," *J. Chem. Phys.* **43**, 1515–1517 (1965).
- <sup>48</sup>J. V. Lill, G. A. Parker, and J. C. Light, "Discrete variable representations and sudden models in quantum scattering theory," *Chem. Phys. Lett.* **89**, 483–489 (1982).
- <sup>49</sup>J. C. Light, I. P. Hamilton, and J. V. Lill, "Generalized discrete variable approximation in quantum mechanics," *J. Chem. Phys.* **82**, 1400–1409 (1985).
- <sup>50</sup>Z. Bačić and J. C. Light, "Theoretical methods for rovibrational states of floppy molecules," *Annu. Rev. Phys. Chem.* **40**, 469–498 (1989).
- <sup>51</sup>V. Szalay, "Discrete variable representations of differential operators," *J. Chem. Phys.* **99**, 1978–1984 (1993).
- <sup>52</sup>J. M. Bowman, T. Carrington, and H.-D. Meyer, "Variational quantum approaches for computing vibrational energies of polyatomic molecules," *Mol. Phys.* **106**, 2145–2182 (2008).
- <sup>53</sup>C. Lanczos, "An iteration method for the solution of the eigenvalue problem of linear differential and integral operators," *J. Res. Natl. Bur. Stand.* **45**, 255–282 (1950).
- <sup>54</sup>G. Brocks, A. van der Avoird, B. T. Sutcliffe, and J. Tennyson, "Quantum dynamics of non-rigid systems comprising two polyatomic fragments," *Mol. Phys.* **50**, 1025–1043 (1983).
- <sup>55</sup>H. G. Kjaergaard, A. L. Garden, G. M. Chaban, R. B. Gerber, D. A. Matthews, and J. F. Stanton, "Calculation of vibrational transition frequencies and intensities in water dimer: Comparison of different vibrational approaches," *J. Phys. Chem. A* **112**, 4324–4335 (2008).
- <sup>56</sup>E. Arunan, G. R. Desiraju, R. A. Klein, J. Sadlej, S. Scheiner, I. Alkorta, D. C. Clary, R. H. Crabtree, J. J. Dannenberg, P. Hobza, H. G. Kjaergaard, A. C. Legon, B. Mennucci, and D. J. Nesbitt, "Definition of the hydrogen bond (IUPAC recommendations 2011)," *Pure Appl. Chem.* **83**, 1637–1641 (2011).
- <sup>57</sup>A. S. Hansen, E. Vogt, and H. G. Kjaergaard, "Gibbs energy of complex formation—combining infrared spectroscopy and vibrational theory," *Int. Rev. Phys. Chem.* **38**(1), 115–148 (2019).
- <sup>58</sup>A. L. Garden, L. Halonen, and H. G. Kjaergaard, "Calculated band profiles of the OH-stretching transitions in water dimer," *J. Phys. Chem. A* **112**(32), 7439–7447 (2008).
- <sup>59</sup>Z. S. Huang and R. E. Miller, "High-resolution near-infrared spectroscopy of water dimer," *J. Chem. Phys.* **91**, 6613–6631 (1989).
- <sup>60</sup>F. Huisken, M. Kaloudis, and A. Kulcke, "Infrared spectroscopy of small size-selected water clusters," *J. Chem. Phys.* **104**, 17–25 (1996).
- <sup>61</sup>J. B. Paul, R. A. Provencal, C. Chapo, K. Roth, R. Casaes, and R. J. Saykally, "Infrared cavity ringdown spectroscopy of the water cluster bending vibrations," *J. Phys. Chem. A* **103**, 2972–2974 (1999).
- <sup>62</sup>U. Buck and F. Huisken, "Infrared spectroscopy of size-selected water and methanol clusters," *Chem. Rev.* **100**, 3863–3890 (2000).
- <sup>63</sup>I. León, R. Montero, F. Castaño, A. Longarte, and J. A. Fernández, "Mass-resolved infrared spectroscopy of complexes without chromophore by nonresonant femtosecond ionization detection," *J. Phys. Chem. A* **116**, 6798–6803 (2012).
- <sup>64</sup>K. E. Otto, Z. Xue, P. Zielke, and M. A. Suhm, "The Raman spectrum of isolated water clusters," *Phys. Chem. Chem. Phys.* **16**, 9849–9858 (2014).

<sup>65</sup>T. A. Ruden, T. Helgaker, P. Jørgensen, and J. Olsen, “Coupled-cluster connected quadruples and quintuples corrections to the harmonic vibrational frequencies and equilibrium bond distances of HF, N<sub>2</sub>, F<sub>2</sub>, and CO,” *J. Chem. Phys.* **121**, 5874–5884 (2004).

<sup>66</sup>G. Rauhut, G. Knizia, and H.-J. Werner, “Accurate calculation of vibrational frequencies using explicitly correlated coupled-cluster theory,” *J. Chem. Phys.* **130**, 054105 (2009).

<sup>67</sup>J. R. Lane and H. G. Kjaergaard, “XH-stretching overtone transitions calculated using explicitly correlated coupled cluster methods,” *J. Chem. Phys.* **132**(17), 174304 (2010).

<sup>68</sup>J. H. Frederick and C. Woywod, “General formulation of the vibrational kinetic energy operator in internal bond-angle coordinates,” *J. Chem. Phys.* **111**, 7255–7271 (1999).